Mon. Not. R. Astron. Soc. **325,** 1411–1430 (2001)

The ATCA intraday variability survey of extragalactic radio sources

L. L. Kedziora-Chudczer,[1,2★†] D. L. Jauncey,[2] M. H. Wieringa,[2] A. K. Tzioumis[2] and J. E. Reynolds[2]

[1]*Special Research Centre for Theoretical Astrophysics, The University of Sydney, NSW 2006, Australia*
[2]*Australia Telescope National Facility, CSIRO, P.O. Box 76, Epping NSW 1710, Australia*

Accepted 2001 March 16. Received 2001 March 16; in original form 2000 July 13

ABSTRACT

We present the results of an Australia Telescope Compact Array (ATCA) survey for intraday variability (IDV) of the total and polarized flux densities of 118 compact, flat-spectrum, extragalactic radio sources from the Parkes 2.7-GHz Survey. A total of 22 total flux density IDV sources were discovered and 15 sources were found to show IDV of their polarized flux density. We discuss the statistical properties of the IDV sources, including the distribution of source modulation indices, and the dependence of the variability amplitude on source spectral index and on Galactic position. We suggest interstellar scintillation (ISS) in the Galactic interstellar medium as the most likely mechanism for IDV. Even so, the inferred high brightness temperatures cannot be easily explained.

Key words: polarization – scattering – ISM: general – galaxies: active – galaxies: nuclei – radio continuum: galaxies.

1 INTRODUCTION

The first systematic investigation of short time-scale variability in a large sample of extragalactic radio sources was carried out by Heeschen (1984). He observed a sample of 226 strong sources ($S_{6\,\mathrm{cm}} \geq 1.0$ Jy) at 9 cm. Most of the compact, flat-spectrum sources in his sample showed significant flux density fluctuations, with an average amplitude of 1.5 per cent on time-scales of 2–20 d. The steep-spectrum radio sources did not appear to vary. This so-called *flickering* was interpreted in terms of refractive scintillations caused by the inhomogeneous structure of the interstellar medium in our Galaxy.

A search for more rapid and possibly stronger flickering through better sampled observations of compact, flat-spectrum radio sources was undertaken by Witzel et al. (1986) and Heeschen et al. (1987) at the 100-m radio telescope of the Max Planck Institut für Radioastronomie (MPIfR). They reported 10 per cent flux density variations at 11 cm in the BL Lac object S5 0716+71 on a time-scale of a day, and they also confirmed the statistical difference in the variability of steep- and flat-spectrum radio sources.

Multi-frequency observations of intraday variable sources at MPIfR and the VLA suggested that the variability tends to be strongest at 2.7 GHz and well correlated between 8 and 2.7 GHz (Wagner & Witzel 1995). Monitoring of the polarized flux density for the two strongest intraday variability (IDV) sources, S5 0716+714 and S5 0917+624, revealed polarization variability correlated with the total flux density fluctuations for S5 0716+714 and anti-correlated for S5 0917+624 (Wegner 1994). Rapid variability in the position angle of the polarized flux density was also reported in these sources (Quirrenbach et al. 1989).

The interest in IDV at cm wavelengths is motivated by the high brightness temperatures inferred from the variability time-scales, well above the $T_{\mathrm{C}} \sim 10^{12}$ K inverse Compton limit (Kellermann & Pauliny-Toth 1969). Possible mechanisms which can lead to IDV fall into two categories, those intrinsic to the source (e.g. shocks in jets, coherent emission) and propagation effects, such as microlensing and interstellar scintillation (ISS, see e.g. the review by Wagner & Witzel 1995). None of the models proposed has been successful in providing a complete description of the observed properties of this phenomenon. It is likely that both extrinsic and intrinsic mechanisms are responsible for the observed rapid flux density fluctuations at cm wavelengths. The present ATCA IDV Survey and monitoring program provides a large, uniform, high-precision, multiwavelength set of observations, which aims to describe the common properties of IDV sources and shed the light on the origin of short-term variations.

2 THE SAMPLE SELECTION

The sample selected for the ATCA survey is drawn from the Parkes–Tidbinbilla Interferometer (PTI) flat-spectrum ($\alpha^{2.7\,\mathrm{GHz}}_{5.0\,\mathrm{GHz}} > -0.5$)[1] survey (Duncan et al. 1993). Sources were chosen which had a ratio of the PTI flux density to total flux density

★E-mail: lkedzior@atnf.csiro.au
†Present address: Anglo-Australian Observatory, PO Box 296, Epping 1710, NSW, Australia.

[1] Hereafter, the spectral index is defined as $S \propto \nu^{\alpha}$ where ν is the frequency of radiation and S is the flux density.

Table 1. List of sources selected for the IDV Survey and the structural information obtained from the closure phases and self-calibration. The columns are labelled as follows: (1) B1950 Parkes Catalogue name, (2, 3) new galactic coordinates: l_{II} longitude and b_{II} latitude calculated from equatorial (1950.0) coordinates, (4) optical identification and (5) redshift obtained from the NASA/IPAC Extragalactic Database (NED), (6) categorizes the sources at a given frequency: 8.6, 4.8, 2.4 and 1.4 GHz (from left to right) according to a percentage of the flux density S_{ext} observed in the ATCA IDV survey (see equation 1). P denotes a point source ($S_{ext} < 0.5$ per cent), C – compact source (0.5 per cent $\leq S_{ext} <$ 3.5 per cent) and E – extended source ($S_{ext} \geq 3.5$ per cent), d indicates an axisymmetric structure and c denotes strong confusing sources in the field. Optical identification abbreviations are as follows: Q – quasar, G – galaxy, HPQ – highly polarized quasar, BL Lac – BL Lacertae type object, EF – empty field, IrS – IRAS source, Sy1 – Seyfert 1 radio galaxy. (*) marks the sources which are known to be optically variable, (†) – obscured field, (§) – large differences in S_{ext} between different observing sessions.

Parkes Source name	Galactic coord. l_{II} (deg)	b_{II} (deg)	ID	z	Source structure			
0003−066	93.21	−66.51	G	0.347	P	P	C	E
0013−005	103.70	−61.75	Q	1.575	C	P	C	C
0023−263	42.26	−84.10	G	0.322	Cd	Cd	P	E
0044−846	303.14	−32.80	Q		P	C	E	E
0048−427	303.70	−74.70	Q	1.749	P	P	C	E
0056−572	301.09	−60.17	Q		C	C	C	Ec
0104−408	290.98	−76.25	Q	0.584	P	P	C	E
0122−003	140.66	−61.75	Q*	1.070	Pc	C	E	E
0131−522	288.25	−63.98	Q		C	C	C	Ec
0138−097	158.45	−68.86	BL Lac*	0.440	E	E	E	E
0142−278	218.02	−78.26	Q	1.153	C	C	C	E
0146+056	147.79	−54.24	Q	2.345	P	P	C	Ec
0150−334	241.26	−75.56	Q	0.610	C	P	C	Cc
0202−172	185.61	−70.31	Q	1.740	P	P	C	Cc
0208−512	276.27	−61.91	HPQ	1.003	C	C	C	C
0214−522	276.14	−60.55	EF		E	E	C	Cc
0215+015	162.07	−54.46	BL Lac*	1.715	P	P	Cc	E
0220−349	239.75	−69.20	Q		P	P	Ec	Ec
0252−549	272.49	−54.61	Q	0.537	C	C	Cc	E
0302−623	280.23	−48.81	Q		C	C	Cc	Cc
0308−611	278.14	−49.06	Q		Cj	C	C	C
0334−546	266.87	−49.62	Q		C	C	C	Ec
0336−019	187.76	−42.63	HPQ*	0.852	P	Cc	C	Ec
0346−279	224.38	−51.02	Q	0.988	C	C	Cc	E
0355−483	256.14	−48.60	Q	1.005	C	C	C	E
0405−385	241.18	−47.93	Q	1.285	P	P	C	C
0420−014	195.12	−33.26	HPQ*	0.915	P	P	C	Ec
0422+004	193.64	−31.87	BL Lac*	0.310	C	C	Ec	E
0426−380	240.63	−43.79	BL Lac	1.030	C	Cc	Ec	Ec
0434−188	216.21	−37.97	Q	2.702	C	C	E	E
0437−454	250.76	−41.85	Q		C	C	E	E
0440−003	197.10	−28.43	Q	0.850	C	C	C	E
0450−469	252.68	−39.57	Q		C	C	C	E
0454−463	251.91	−38.88	Q	0.850	E	E	E	E
0454−810	293.75	−31.42	Q	0.444	P	P	P	C
0457+024	197.00	−23.40	Q	2.384	P	P	P	C
0502+049	195.40	−21.03	Q		C	C	Ec	E
0522−611	270.14	−34.19	Q	1.400	C	C	C	Ec
0528−250	228.19	−28.23	Q*	2.779	C	P	C	E
0537−286	232.77	−27.46	Q	3.104	C	C	E	E
0537−441	250.06	−31.15	BL Lac*	0.894	P	Pc	Cc	Cc
0607−157	222.57	−16.28	Q	0.324	P	P	Ec	C
0642−349	244.20	−16.59	Q	2.165	C	C	C	Ec
0646−306	240.43	−14.14	Q	0.455	P	P	C	C
0648−165	227.63	−7.72	EF†		P	P	E	E
0727−115	227.58	2.97	EF†		P	C	C	C

Table 1 – *continued*

Parkes Source name	Galactic coord. l_{II} (deg)	b_{II} (deg)	ID	z	Source structure			
0728−320	245.70	−6.68	Q		C	P	E	E
0733−174	233.45	1.38	EF†		C	P	P	C
0736+017	216.94	11.21	HPQ*	0.191	P	P	C	P
0808+019	220.63	18.37	BL Lac*		Ed§	P	C	E
0829+046	220.73	24.26	BL Lac*	0.180	P	P	Cc	Ec
0834−201	243.51	12.16	Q	2.752	P	C	C	E
0837+035	222.85	25.49	BL Lac		C	C	C	E
1021−006	245.05	44.76	Q*	2.547	C	C	Cc	Ec
1034−293	270.76	24.74	BL Lac	0.312	P	C	E	E
1036−154	261.94	36.41	Q		C	C	E	E
1048−313	274.74	24.60	EF		C	P	C	C
1057−797	297.93	−18.22	Q		P	P	Cc	C
1105−680	293.47	−7.34	Q	0.588	P	C	C	E
1115−122	270.00	44.31	Q/IrS		C	C	C	E
1127−145	275.07	43.62	Q	1.187	Ed	Pc§	Cc	Cc
1143−245	284.44	35.72	Q	1.950	E	C	C	E
1144−379	289.13	22.95	BL Lac*	1.048	P	Pc	C	E
1148−001	272.44	58.84	Q*	1.976	P	P	C	Ec
1148−671	297.10	−5.20	Q		P	C	E	C
1243−072	300.38	55.37	Q	1.286	P	C	C	C
1253−055	304.83	57.09	HPQ*	0.538	C	P	E	E
1255−316	304.49	30.98	Q	1.924	P	C	C	E
1256−220	305.14	40.57	Q	1.306	C	C§	C	E
1334−127	319.67	48.44	BL Lac*	0.539	P	C	C	C
1351−018	332.55	57.21	Q	3.707	C	C	C	E
1354−152	325.28	44.58	Q	1.890	C	C	C	Ec
1402−012	337.50	56.44	Q*	2.518	C	C	C	E
1406−076	333.81	50.35	Q	1.494	P	C	E	E
1435−218	333.19	34.53	Q	1.194	C	C	Cc	E
1443−162	338.77	38.38	Q		C	C	E	E
1502+036	2.03	50.34	Q	0.411	C	P	C	E
1504−166	343.64	35.17	HPQ*	0.876	P	P	C	E
1519−273	339.48	24.51	BL Lac		P	C	C	C
1535+004	5.94	41.92	EF		P	C	C	E
1540−828	308.27	−22.02	EF		C	P	C	C
1549−790	311.22	−19.39	G	0.15	P	Cc	P	E
1555−140	356.43	28.79	GPair	0.097	C	C	C	E
1556−245	348.33	21.27	Q	2.813	C	C	E	E
1610−771	313.45	−18.77	Q*	1.710	P	P	Cc	Ec
1619−680	320.76	−12.96	Q	1.360	P	C	C	Ec
1622−297	348.71	13.50	Q	0.815	P§	P	Cc	C
1718−649	326.98	−15.73	G	0.014	P	P	Pc	C
1741−038	21.56	13.21	HPQ	1.054	P	C	P	C
1758−651	328.84	−19.57	G		P	P	C	C
1815−553	339.22	−17.68	Q		P	P	C	E
1921−293	9.32	−19.45	HPQ*	0.352	P	P	Pc	Pc
1925−610	335.85	−28.02	Q		P	C	C	E
1937−101	29.35	−15.21	Q	3.780	C	P	C	E
1958−179	24.06	−23.08	Q	0.650	P	C	C	C
2016−615	335.38	−34.15	Q		C	C	C	E
2052−474	352.65	−40.24	Q	1.489	Cc	Cc	Ec	Ec
2058−297	15.86	−39.76	Q	0.698	C	P	C	E
2106−413	0.78	−42.77	Q	1.055	P	C	C	C
2109−811	311.62	−32.24	EF		C	P	C	E
2121+053	57.89	−30.12	Q	1.878	P	P	C	C
2126−158	35.95	−41.74	Q	3.268	P	P	C	E
2128−123	40.46	−40.75	Sy1*	0.501	P	C	C	C
2134+004	55.38	−35.60	Q*	1.932	P	P	P	E

Table 1 – *continued*

Parkes Source name	Galactic coord. l_{II} (deg)	b_{II} (deg)	ID	z	Source structure			
2142−758	315.85	−36.54	Q	1.139	C	C	C	E
2146−783	313.24	−35.19	Q		C	C	E	E
2149−307	17.08	−50.78	Q	2.345	C	C	C	C
2155−304	17.80	−52.03	BL Lac*	0.116	C	P	C	E
2243−123	53.83	−56.89	Q*	0.630	P	C	C	C
2245−328	13.96	−62.74	Q	2.268	C	C	E	E
2312−319	15.05	−68.50	Q	0.284	C	C	C	E
2320−035	77.46	−58.02	Q	1.411	P	C	C	C
2326−477	336.01	−64.04	Q	1.299	C	C	C	Cc
2329−384	354.58	−70.00	Q	1.195	C	C	C	E
2332−017	84.07	−58.37	Q*	1.185	C	P	E	E
2333−528	326.90	−60.94	Q		P	C	Cc	E
2345−167	65.56	−71.74	HPQ*	0.576	C	P	C	C
2355−534	320.33	−62.15	Q*	1.006	P	P	E	C

larger than 0.9. Flat-spectrum, compact components of radio sources are usually self-absorbed and coincide with the optical quasar or active galactic nucleus (AGN, e.g. Jauncey et al. 1982). We chose such sources because (i) monitoring of flux density with an interferometer such as the ATCA can be done faster and more accurately for unresolved sources, and (ii) it is known from previous studies (e.g. Heeschen et al. 1987) that flat-spectrum sources are more likely to show IDV than steep-spectrum sources.

The final sample contains 118 sources, randomly distributed over the southern sky for $b < 10°$. They are listed in Table 1 along with identifications, galactic coordinates, redshift and measured source structure information. The sample contains 90 (76 per cent) quasars, 13 (11 per cent) BL Lacs, 7 (6 per cent) galaxies and 8 (7 per cent) unidentified sources.

3 OBSERVATIONS

The main objective of the Survey was to obtain well-sampled, multifrequency total and polarized flux density measurements for all sources in the sample within the 96 h scheduled for each observing run. Our observations were carried out at the ATCA, an east–west earth-rotation synthesis interferometer, with six 22-m antennas on a 6-km baseline (Sinclair & Gough 1991). The ATCA has a number of desirable features for a study of short time-scale variability:

(i) short integration time which enables frequent sampling,
(ii) broad-band instantaneous frequency coverage,
(iii) the high accuracy and sensitivity essential to monitor polarization and to explore the low-amplitude 'flicker' of extra-galactic sources.

During the two observing sessions in 1994 May and August, the flux densities of sources in the sample were measured every 2 h at the four ATCA frequencies, 1.4, 2.4, 4.8 and 8.6 GHz. We used PKS 1934−638 as the primary flux density calibrator. Additionally, the known steep-spectrum sources PKS 0518+165, PKS 0134+329, PKS 1328+307 and PKS 0823−500 were observed throughout each session to check the overall gain stability and calibration.

The observations were performed in continuum mode with 128-MHz bandwidth divided into 32 channels. This configuration enables measurements of four polarization products for each frequency. The sampling time was chosen to be 1 min, which is equivalent to six 10-s integrations on source. To avoid long slew times, the sources were observed in two main groups, either north or south of zenith. Each group was observed over 24 h, with each source being observed every 2 h while it was above 20° elevation. The flux density of each source, including calibrators, was measured typically 6 times over 12 h, and the measurements repeated in the same way 36 h later.

Table 2. The normalized scatter of PKS 1934 − 638 flux density measurements ($\mu_{1934-638}$), averaged over two observing runs, 1994 May and August, at each of the four ATCA frequencies.

frequency (GHz)	$\mu_{1934-638}$ (%)	theoretical rms in 1 min observation (mJy)	measured rms (mJy)
8.6	0.35	0.67	2.4
4.8	0.24	0.72	1.8
2.4	0.50	0.76	3.9
1.4	0.41	0.60	3.8

The gain stability was monitored by regular observations of PKS 1934−638 and the other non-variable sources, and so the scatter in their measured flux densities is an estimate of the uncertainties in the individual flux density measurements. This includes the effects of antenna pointing errors and gain changes with elevation and time.

The telescope pointing, typically 7 arcsec rms, was determined before each observing session. The positions of all sample sources are known to an accuracy of 0.5 arcsec or better, so that flux density errors caused by mis-pointing do not exceed 0.1 per cent at the highest frequencies. The observed rms errors for the primary flux density calibrator, PKS 1934−638, for an individual 1-min observing scan are listed in Table 2 for each frequency. Thus, at the flux density limit, $S \geq 0.5$ Jy, the gain stability and pointing errors dominate, while the thermal noise is typically less than a mJy.

The source structure information presented in columns 6–9 of Table 1 is derived from the closure phase estimates (Jennison 1958) of the possible extended component in the measured flux density given by

$$S_{\rm ext} = C\bar{S}(\sigma^2_{\rm obs} - \sigma^2_{\rm theo})^{1/2}, \quad (1)$$

where $\bar{S}$ is the flux density averaged over 12 h, $\sigma_{\rm obs}$ is the observed

rms of closure phases measured for all independent baselines and $\sigma_{\rm theo}$ is a theoretically predicted rms of closure phases for a point source calculated by use of calibration from antenna noise diodes (Sault, private communication). C is a constant of the order of unity.

We find that most of the target sources of the ATCA IDV Survey are unresolved at 8.6 and 4.8 GHz. In particular, 72 per cent of the sample sources show less than 1 per cent extended flux density at 4.8 GHz. However only 22 per cent and 5 per cent of the sources at 2.4 and 1.4 GHz respectively satisfy this condition (Table 1).

Almost half of the sample (62 sources) shows more than 5 per cent flux density in an extended component at 1.4 GHz. The effects of weak extended structure and confusing sources in the primary beam result in much larger object-dependent flux density errors at this frequency. Therefore the results of the 1.4-GHz measurements are excluded from the statistical discussion of the survey.

4 RESULTS

4.1 Flux densities

The results of the Survey are presented in Tables 3 and 4, which show the averaged total ($\bar{S}$) and polarized ($\bar{P}$) flux densities, averaged polarization position angles (ψ) and the corresponding modulation indices ($\mu_{\bar{S}}$, $\mu_{\bar{P}}$).

The total flux densities in Table 3 are the averages of all 1-min measurements within a given observing session over typically 96 h. In each session the number of data points, N, used in the averages ranges between 5 and 36 with a median of 11. Each data point used to obtain the flux density in Table 3 is an average over all ATCA baselines of typically six 10-s integrations.

Seven sources (PKS 0023−263, PKS 0122−003, PKS 0138−097, PKS 208−512, PKS 0454−463, PKS 1253−055 and PKS 2052−474) were excluded from the sample because of the presence of either extended structure at all frequencies or strong confusing sources in the primary beam. A further 36 sources were found to be confused, or in a few cases, extended at 2.4 and 1.4 GHz. These have blank entries in Tables 3 and 4 at the corresponding frequencies. In this way the consistently high-quality data at high frequencies was maintained by reducing the size of the sample slightly. The final numbers of sources at each frequency in the Table 3 are 111 for 8.6 GHz, 105 for 4.8 GHz, 74 for 2.4 GHz and 55 for 1.4 GHz.

The 1.4-GHz data was not used in the IDV investigation, although the average flux densities have been retained in both tables for the sources with $S_{\rm ext} \geq 3.5$ per cent.

The errors in the observed flux densities in Tables 3 and 4 have been determined from the observed scatter in the strong sources. Table 2 shows the observed scatter for the primary flux density calibrator PKS 1934−638, the non-variable point source most frequently observed throughout each Survey session. The measured rms noise integrated over 1 min never exceeds 4 mJy. With normalized flux density errors of no more than 0.5 per cent at each of the four frequencies, the present accuracy compares favourably with the precision of single-dish measurements.

The ATCA antennas each have two, on-axis, orthogonal, linearly polarized feeds at all frequencies, which enable easy acquisition of all Stokes parameters. The polarized flux densities P, and the position angles, ψ, along with the modulation indices, μ_P, are presented for the 74 sources with $P > 15$ mJy in Table 4. The degree of linear polarization observed for compact, flat-spectrum, synchrotron sources is typically a small fraction of the total flux density (≤5 per cent) (Aller at al. 1985), and this is the case for the majority of sources observed in the present Survey (Fig. 1).

Monitoring sessions in 1994 May and August provided two data sets of the same sample. To determine whether the data obtained in 1994 May and August are comparable in the statistical sense, we applied the Kolmogorov–Smirnov test for the source number distributions of normalized standard deviations or modulation indices, $\mu\,(=\sigma_S/\bar{S})$ of the flux density measurements. This found no statistically significant difference between the 1994 May and August results at the confidence level 0.05 per cent.

4.2 Spectral index properties

The average spectral indices: $\alpha^{8.6}_{4.8}$, $\alpha^{4.8}_{2.4}$, $\alpha^{2.4}_{1.4}$ and $\alpha^{8.6}_{1.4}$ are listed in Table 5. The uncertainty of the spectral index measurement depends on the modulation indices at the relevant frequencies and on the ratio of these frequencies. The estimated $\sigma_\alpha \sim 2$ per cent for non-variable sources is slightly dependent on the frequency pair used.

The distribution of the spectral indices $\alpha^{4.8}_{2.4}$ is shown in Fig. 2. There are only three sources with $\alpha^{4.8}_{2.4} \leq -0.5$. If spectral indices $\alpha^{4.8}_{2.4}$ are compared with indices $\alpha^{5.0}_{2.7}$ measured with the Parkes telescope, it is evident that, while the sources may vary considerably, very few, if any of the original flat-spectrum sources change to steep-spectrum sources (Fig. 2b). The differences in the distribution of spectral indices between 1994 May and August (Fig. 2a) reflect the level of monthly variability of the flat-spectrum sources.

The flat-spectrum sources ($\alpha^{5.0}_{2.7} \geq -0.5$) remain flat-spectrum over much longer time-scales, which is illustrated in the scatter plots of average flux densities shown for the increasing time difference between measurements (Fig. 3).

The shapes of our four-frequency spectra can be described as decreasing with frequency, straight, peaked, concave, inverted and complex. The largest population represented in the Survey sample (42 sources corresponding to 36 per cent) are peaked-spectrum sources. The second largest groups are 22 (19 per cent) decreasing- and 21 (18 per cent) inverted-spectrum sources. There are three (2.5 per cent) sources with a straight spectrum (with <50 mJy deviations from an $\alpha = 0$ line), 11 (9.3 per cent) concave-spectrum and one (0.8 per cent) complex-spectrum source.

The shape of the spectrum changed for the 15 per cent of sources between two observing sessions. Interestingly, no transition from peaked to concave spectrum was observed. This may suggest that, at the typical time-scale of months, the flux density changes are caused by the slower 'van der Laan-type' evolution corresponding to the physical expansion of the region of the original outburst (van der Laan 1966).

4.3 Short-term variability

The normalized amplitude of variability is expressed in terms of a modulation index, μ, calculated over 96 h, the duration of each observing session. Fig. 3 illustrates the different time-scales of flux density variations in our sample by comparing measurements obtained 1 day apart, 3 months apart and a few decades apart. While large flux-density fluctuations over the short (day-to-day) time-scales are rare in an ensemble of flat-spectrum, compact sources it is clear that all these sources vary significantly on a time-scale of decades.

The number distribution of modulation indices is shown in Fig. 4. The peaks in these distributions give an independent estimate of the normalized rms error in our measurements of flux densities. If one

Table 3. The averaged total flux densities ($\bar{S}$) and the modulation indices ($\mu_{\bar{S}}$) for the sample of IDV sources. N is the number of data points included in averages. The subscripts (1) and (2) correspond to measurements for two different observing runs: 1994 May and August. The table shows the data for four frequencies: 8.6 GHz, 4.8 GHz, 2.4 GHz and 1.4 GHz.

	8.6 GHz						4.8 GHz						2.4 GHz						1.4 GHz					
	94 May			94 August			94 May			94 August			94 May			94 August			94 May			94 August		
Source name	N	$\bar{S}_1$ Jy	$\mu_{\bar{S}_1}$	N	$\bar{S}_2$ Jy	$\mu_{\bar{S}_2}$	N	$\bar{S}_1$ Jy	$\mu_{\bar{S}_1}$	N	$\bar{S}_2$ Jy	$\mu_{\bar{S}_2}$	N	$\bar{S}_1$ Jy	$\mu_{\bar{S}_1}$	N	$\bar{S}_2$ Jy	$\mu_{\bar{S}_2}$	N	$\bar{S}_1$ Jy	$\mu_{\bar{S}_1}$	N	$\bar{S}_2$ Jy	$\mu_{\bar{S}_2}$
0003−066	16	3.06	0.006	7	2.85	0.003	16	3.17	0.005	7	3.08	0.004												
0013−005	9	0.83	0.009	7	0.84	0.004	9	1.01	0.006	7	1.08	0.003	13	1.11	0.008	7	1.16	0.013	13	1.06	0.009	7	1.09	0.007
0044−846	15	0.50	0.008				15	0.013	0.035															
0048−427	16	1.06	0.007	8	1.07	0.004	17	0.92	0.006	8	0.99	0.005												
0056−572	13	0.52	0.006	12	0.50	0.008	13	0.58	0.008	12	0.57	0.007												
0104−408	17	2.60	0.011	9	3.03	0.003	17	1.55	0.013	9	1.80	0.004	13	0.91	0.044	9	0.93	0.007						
0131−522	13	0.47	0.008				13	0.010	0.038				17	0.38	0.010									
0142−278	9	0.72	0.010	10	0.62	0.005	9	0.76	0.011	10	0.74	0.007	9	0.71	0.010	10	0.73	0.010						
0146+056	9	1.25	0.004	7	1.27	0.005	9	1.32	0.006	7	1.36	0.003	7	1.07	0.013	7	1.10	0.011	7	0.81	0.020	7	0.84	0.012
0150−334	17	0.89	0.006	10	0.82	0.004	17	1.05	0.007	10	1.01	0.003	12	1.11	0.017	9	1.10	0.008	12	1.12	0.017	9	1.13	0.012
0202−172	9	1.45	0.017	10	1.42	0.008	9	1.42	0.007	10	1.47	0.009	11	1.23	0.024	10	1.26	0.008	11	1.18	0.017	10	1.19	0.018
0214−522	21	0.34	0.008	10	0.33	0.004	21	0.51	0.004	10	0.51	0.005	14	0.71	0.009	11	0.72	0.010	14	0.86	0.008	11	0.87	0.013
0215+015	10	0.71	0.007	9	0.84	0.010	10	0.56	0.014	9	0.68	0.008	7	0.55	0.021	9	0.56	0.018						
0220−349	13	0.80	0.010	14	0.81	0.005	13	0.83	0.007	14	0.85	0.005	16	0.74	0.020	10	0.73	0.005	16	0.69	0.019	10	0.65	0.017
0252−549	17	0.94	0.008																					
0302−623	12	1.89	0.003	12	1.86	0.006	12	2.09	0.007	12	2.08	0.004	18	2.13	0.009	13	2.10	0.008	18	2.16	0.009	13	1.93	0.005
0308−611	14	1.67	0.008	15	1.72	0.017	14	1.36	0.014	15	1.46	0.011							11	0.90	0.024	12	0.94	0.016
0334−546	12	0.39	0.004	11	0.37	0.004	12	0.52	0.005	11	0.50	0.005	14	0.49	0.007	16	0.48	0.005	14	0.38	0.016	16	0.37	0.035
0336−019	7	2.50	0.012	8	2.34	0.009																		
0346−279	9	1.25	0.009	11	1.08	0.007	9	1.22	0.030	11	1.01	0.015	7	1.05	0.016	11	0.90	0.022	7	0.96	0.027	10	0.81	0.030
0355−483	13	0.35	0.005	34	0.35	0.038	13	0.46	0.009	34	0.46	0.005	11	0.40	0.017	35	0.41	0.009						
0405−385	11	1.45	0.043	76	1.33	0.003	11	1.38	0.056	76	1.27	0.007	14	1.13	0.056	77	1.08	0.011	14	0.92	0.052	77	0.90	0.009
0420−014	6	2.27	0.012	11	2.10	0.011	6	2.45	0.006	11	2.28	0.005	6	2.37	0.007	15	2.50	0.008	6	2.02	0.013	14	2.69	0.011
0422+004	10	0.51	0.018				10	0.024	0.068															
0426−380	15	1.44	0.008	22	1.62	0.004																		
0434−188	8	0.98	0.010	13	0.97	0.007	8	1.07	0.013	13	1.06	0.007												
0437−454	11	0.32	0.025	35	0.34	0.009	10	0.33	0.016	35	0.33	0.014												
0440−003				11	0.029	0.059				11	1.68	0.011				11	0.018	0.043				10	1.48	0.015
0450−469	15	0.34	0.012	21	0.42	0.003	15	0.41	0.016	21	0.48	0.004	11	0.46	0.034	24	0.49	0.006						
0454−810	16	1.87	0.014	17	2.03	0.006	16	1.72	0.019	17	1.79	0.010							13	1.28	0.010	17	1.16	0.012
0457+024	7	1.30	0.007	12	1.31	0.011	7	1.75	0.007	12	1.80	0.009	7	2.00	0.013	10	2.05	0.025	7	1.94	0.014	9	1.97	0.029
0502+049	6	0.64	0.005	9	0.72	0.027	6	0.81	0.018	9	0.77	0.011							10	0.91	0.024	8	0.85	0.021
0522−611	11	0.65	0.007	13	0.61	0.008	11	0.66	0.005	13	0.65	0.007	15	0.67	0.010	14	0.69	0.007	15	0.73	0.015	13	0.75	0.022
0528−250	8	0.63	0.020	14	0.63	0.009	8	0.86	0.014	14	0.86	0.005												
0537−286	8	0.45	0.007	13	0.39	0.006	8	0.67	0.018	13	0.56	0.005												
0537−441	12	6.43	0.006	35	6.29	0.004																		
0607−157	10	4.02	0.012	11	5.74	0.005	10	3.20	0.013	12	4.15	0.023	8	2.40	0.013	11	2.80	0.031	8	2.43	0.009	10	2.61	0.008
0642−349	16	0.79	0.008	11	0.77	0.009	16	0.94	0.007	11	0.93	0.011	11	0.82	0.019	12	0.82	0.010	11	0.73	0.026	12	0.73	0.020
0646−306	11	1.08	0.014	16	0.99	0.012	11	1.10	0.024	16	1.05	0.011	13	0.82	0.037	11	0.91	0.024	13	0.76	0.021	11	0.76	0.032
0648−165	10	1.52	0.009	12	1.64	0.007	10	1.47	0.008	12	1.52	0.009												

Table 3 – *continued*

Source name	8.6 GHz 94 May N	$\bar{S}_1$ Jy	$\mu_{\bar{S}_1}$	8.6 GHz 94 August N	$\bar{S}_2$ Jy	$\mu_{\bar{S}_2}$	4.8 GHz 94 May N	$\bar{S}_1$ Jy	$\mu_{\bar{S}_1}$	4.8 GHz 94 August N	$\bar{S}_2$ Jy	$\mu_{\bar{S}_2}$	2.4 GHz 94 May N	$\bar{S}_1$ Jy	$\mu_{\bar{S}_1}$	2.4 GHz 94 August N	$\bar{S}_2$ Jy	$\mu_{\bar{S}_2}$	1.4 GHz 94 May N	$\bar{S}_1$ Jy	$\mu_{\bar{S}_1}$	1.4 GHz 94 August N	$\bar{S}_2$ Jy	$\mu_{\bar{S}_2}$
0727−115	13	4.86	0.005	12	4.18	0.007	13	5.09	0.012	12	4.34	0.007	10	3.97	0.009	14	3.69	0.011	10	3.27	0.013	13	2.90	0.013
0728−320	13	0.23	0.026	11	0.22	0.011	13	0.31	0.034	11	0.33	0.007												
0733−174	9	1.31	0.010	12	1.29	0.004	9	1.88	0.004	12	1.84	0.007	13	2.59	0.012	15	2.47	0.011	13	2.74	0.006	15	2.72	0.004
0736+017	9	1.32	0.012	13	1.03	0.019	9	1.41	0.013	13	1.22	0.012	8	1.53	0.013	10	1.65	0.022	8	1.75	0.010	10	2.02	0.010
0808+019	9	1.02	0.014	12	0.57	0.021	9	0.97	0.011	12	0.59	0.023	13	0.80	0.025	13	0.56	0.022						
0829+046	11	1.18	0.007	11	1.23	0.007	11	1.12	0.000	11	1.10	0.013	8	1.00	0.004	12	0.98	0.016	8	0.97	0.016	12	0.93	0.017
0834−201	10	2.24	0.013	12	2.13	0.010	10	1.84	0.004	12	1.75	0.005	14	1.64	0.011	13	1.62	0.012						
0837+035	9	0.69	0.014	11	0.68	0.007	9	0.75	0.004	11	0.74	0.012	8	0.71	0.016	10	0.72	0.011						
1021−006	9	0.52	0.009	7	0.51	0.003	9	0.77	0.008	7	0.76	0.005	12	1.01	0.007	8	1.03	0.008	12	0.99	0.015	6	1.01	0.017
1034−293	11	1.80	0.057	10	2.32	0.012	11	1.17	0.092	10	1.78	0.113												
1036−154	9	0.41	0.013	11	0.41	0.007	9	0.39	0.006	11	0.39	0.007												
1048−313	15	0.73	0.026	10	0.72	0.019	15	0.87	0.011	10	0.86	0.025	11	0.91	0.023	9	0.94	0.010	11	0.85	0.030	9	0.93	0.015
1057−797	11	2.10	0.007	15	2.09	0.009	14	1.49	0.002	19	1.33	0.014	14	1.01	0.010	17	1.04	0.015						
1105−680	12	1.04	0.008	15	1.01	0.007	12	1.20	0.003	16	1.22	0.004	11	0.92	0.010	14	1.00	0.009						
1115−122	11	0.68	0.019	9	0.59	0.003	11	0.65	0.018	9	0.58	0.012	9	0.62	0.009	9	0.61	0.013						
1127−145	9	2.84	0.005	9	2.82	0.005	9	3.57	0.003	9	3.58	0.003	13	4.39	0.008	11	4.50	0.013	12	5.06	0.007	9	5.19	0.007
1143−245	17	1.03	0.008	10	1.03	0.006	17	1.43	0.003	10	1.40	0.004	10	1.68	0.010	11	1.66	0.013						
1144−379	12	2.33	0.075	9	2.14	0.017	12	2.47	0.146	9	2.04	0.031												
1148−001	9	1.16	0.006	9	1.14	0.002	9	1.61	0.002	9	1.58	0.002	11	2.14	0.005	8	2.19	0.004	11	2.63	0.004	8	2.64	0.009
1148−671	13	1.15	0.005	15	1.11	0.009	13	1.69	0.006	15	1.66	0.002							12	1.29	0.017	12	1.10	0.013
1243−072	14	1.08	0.007	6	1.06	0.006	14	0.87	0.007	6	0.86	0.001	11	0.63	0.004	7	0.66	0.003	11	0.54	0.012	7	0.55	0.018
1255−316	15	1.47	0.009	8	1.47	0.013	15	1.55	0.016	8	1.56	0.009							18	1.12	0.020	11	0.98	0.017
1256−220	16	0.60	0.012	7	0.74	0.027	16	0.52	0.014	7	0.56	0.022	11	0.56	0.009	7	0.57	0.007	11	0.64	0.040	7	0.66	0.017
1334−127	10	5.27	0.008	7	4.88	0.019																		
1351−018	14	0.85	0.007	6	0.84	0.009	14	0.98	0.003	6	0.96	0.014	11	0.82	0.018	6	0.83	0.014						
1354−152	11	0.88	0.007	7	0.84	0.009	11	0.96	0.004	7	0.87	0.010	14	0.76	0.013	7	0.75	0.008						
1402−012	14	0.23	0.013	7	0.23	0.009	14	0.34	0.007	7	0.33	0.005	11	0.43	0.017	7	0.43	0.018	11	0.50	0.027	7	0.48	0.014
1406−076	11	1.01	0.011	7	1.00	0.010	11	0.76	0.010	7	0.80	0.011												
1435−218	14	0.57	0.008	8	0.56	0.010	14	0.63	0.004	8	0.58	0.007												
1443−162	12	0.44	0.012	7	0.39	0.019	12	0.43	0.015	7	0.40	0.008												
1502+036	13	0.60	0.020	6	0.71	0.002	13	0.57	0.014	6	0.66	0.008												
1504−166	12	2.54	0.016	7	2.49	0.004	12	2.71	0.019	7	2.64	0.008												
1519−273	15	1.41	0.029	7	1.77	0.018	15	1.44	0.037	7	1.72	0.023	10	1.09	0.040	8	1.28	0.009	10	0.98	0.035	8	0.91	0.009
1535+004	10	0.43	0.007	7	0.42	0.003	10	0.56	0.004	7	0.55	0.006	15	0.64	0.009	7	0.63	0.009	15	0.68	0.014	7	0.65	0.018
1540−828	15	0.58	0.007	15	0.58	0.004	15	0.67	0.008	15	0.68	0.005	16	0.74	0.005	15	0.74	0.008	16	0.89	0.013	15	0.85	0.026
1549−790	22	3.01	0.003										14	0.002	0.068				14	5.47	0.009			
1555−140	9	0.41	0.015	8	0.41	0.004	9	0.59	0.007	8	0.58	0.004	9	0.65	0.006	7	0.66	0.009						
1556−245	9	0.27	0.015	8	0.28	0.042	9	0.38	0.028	8	0.39	0.033												
1610−771	16	3.17	0.005	13	3.27	0.004	16	3.19	0.005	13	3.25	0.006												
1619−680	24	1.41	0.004	9	1.34	0.003	23	1.93	0.002	9	1.86	0.003	16	2.04	0.006	9	1.88	0.007	16	1.66	0.012	9	1.54	0.009

Table 3 – *continued*

	8.6 GHz						4.8 GHz						2.4 GHz						1.4 GHz					
	94 May			94 August			94 May			94 August			94 May			94 August			94 May			94 August		
Source name	N	$\bar{S}_1$ Jy	$\mu_{\bar{S}_1}$	N	$\bar{S}_2$ Jy	$\mu_{\bar{S}_2}$	N	$\bar{S}_1$ Jy	$\mu_{\bar{S}_1}$	N	$\bar{S}_2$ Jy	$\mu_{\bar{S}_2}$	N	$\bar{S}_1$ Jy	$\mu_{\bar{S}_1}$	N	$\bar{S}_2$ Jy	$\mu_{\bar{S}_2}$	N	$\bar{S}_1$ Jy	$\mu_{\bar{S}_1}$	N	$\bar{S}_2$ Jy	$\mu_{\bar{S}_2}$
1622−297	11	2.25	0.020	10	2.19	0.031	11	2.32	0.011	10	2.24	0.014	10	2.12	0.021	9	2.09	0.016						
1718−649	14	3.60	0.003	9	3.42	0.004	14	4.42	0.002	9	4.33	0.004	17	4.14	0.000	9	4.10	0.006	18	3.47	0.004	9	3.41	0.005
1741−038	11	3.23	0.009	6	3.81	0.006	11	2.53	0.010	6	2.74	0.012	13	1.89	0.014	6	1.94	0.009	13	1.56	0.010	6	1.47	0.005
1758−651	20	0.70	0.007	8	0.67	0.004	20	0.66	0.019	8	0.63	0.005	14	0.61	0.008	9	0.58	0.011	14	0.69	0.009	9	0.65	0.026
1815−553	14	1.10	0.006	8	0.92	0.003	14	1.17	0.004	8	1.01	0.003	17	0.97	0.008	6	1.05	0.008						
1921−293	12	23.9	0.008	11	20.9	0.006	12	19.68	0.006	11	18.06	0.004	9	12.94	0.010	10	13.45	0.008	9	11.28	0.011	8	11.70	0.011
1925−610	8	0.98	0.010	7	0.91	0.006	12	0.96	0.011	7	0.95	0.004	21	0.74	0.015	7	0.76	0.012	21	0.69	0.013	7	0.70	0.011
1937−101	9	0.59	0.012	6	0.60	0.008	8	0.73	0.007	6	0.76	0.005	12	0.86	0.012	7	0.86	0.011	12	0.87	0.008	7	0.80	0.010
1958−179	9	1.17	0.013	6	0.66	0.004	9	1.42	0.010	6	0.72	0.004	8	1.67	0.007	6	0.88	0.006						
2016−615	19	0.33	0.008				19	0.005	0.020				12	0.70	0.012									
2058−297	8	0.60	0.009	8	0.61	0.005	8	0.70	0.007	8	0.68	0.004	9	0.71	0.005	8	0.66	0.004	9	0.53	0.005	8	0.63	0.016
2106−413	9	2.46	0.007	11	2.29	0.005	9	2.15	0.003	11	2.16	0.005	10	1.80	0.007	7	1.74	0.007	10	1.72	0.013	7	1.64	0.010
2109−811				15	0.60	0.006				15	0.61	0.008				16	0.54	0.007				8	0.46	0.021
2121+053	11	1.03	0.008	5	0.97	0.014	11	1.25	0.010	5	1.14	0.010	9	1.34	0.013	5	1.16	0.007	9	1.33	0.012	5	1.07	0.015
2126−158	9	0.97	0.003	7	0.96	0.005	9	1.19	0.004	7	1.19	0.004	9	0.90	0.010	11	0.92	0.007						
2128−123	10	2.55	0.005	8	2.63	0.005	10	2.31	0.007	8	2.27	0.004	9	1.87	0.006	7	1.79	0.007	9	1.57	0.009	7	1.49	0.007
2134+004				7	0.005	0.016				7	8.91	0.004				7	0.006	0.016				7	3.43	0.003
2142−758	13	0.70	0.008	12	0.70	0.007	13	0.87	0.009	12	0.87	0.005												
2146−783	17	0.82	0.005	12	0.79	0.003	17	1.10	0.005	12	1.08	0.004												
2149−307	12	1.50	0.014	6	1.32	0.006	12	1.71	0.010	6	1.62	0.005	17	1.39	0.016	6	1.41	0.016	17	1.16	0.013	6	1.18	0.018
2155−304	20	0.43	0.024	6	0.49	0.008	21	0.44	0.021	6	0.50	0.005	20	0.41	0.034	9	0.47	0.020						
2243−123	14	2.43	0.005	7	2.32	0.003	14	2.35	0.003	7	2.25	0.005	11	1.95	0.016	7	1.90	0.008	11	1.78	0.014	7	1.76	0.012
2245−328	11	0.56	0.008				11	0.010	0.034															
2312−319	9	0.44	0.006	8	0.42	0.008	9	0.58	0.007	8	0.56	0.005	12	0.74	0.011	7	0.74	0.009						
2320−035	9	0.76	0.010	8	0.76	0.007	9	0.80	0.005	7	0.83	0.010	11	0.81	0.010	9	0.83	0.007	11	0.85	0.009	9	0.84	0.011
2326−477	16	1.67	0.006	8	1.62	0.006	16	1.74	0.007	8	1.71	0.010	13	2.13	0.007	9	2.10	0.009	13	2.56	0.013	8	2.55	0.027
2329−384	10	0.48	0.006				10	0.007	0.021				18	0.64	0.007									
2332−017	11	0.55	0.004	7	0.52	0.007	11	0.64	0.009	7	0.62	0.011												
2333−528	16	1.30	0.008	9	1.28	0.005	16	1.54	0.004	9	1.55	0.002	12	1.72	0.010	8	1.73	0.008						
2345−167	11	2.73	0.009	7	3.06	0.002	11	3.01	0.007	7	3.18	0.005							13	2.44	0.007	7	2.50	0.013
2355−534	14	1.66	0.009	8	1.61	0.006	14	1.76	0.005	8	1.76	0.004												

approximates each distribution by a Gaussian plus a tail of high modulation indices, the typical measurement rms values for the frequencies 8.6, 4.8, 2.4 and 1.4 GHz are 0.65, 0.6, 0.8 and 1.2 per cent respectively. The increased rms distribution of modulation indices at 1.4 GHz is the result of confusion and weak extended components present in the sources (as noted in Section 3).

Those sources found in the tails of modulation indices distributions at different frequencies (Fig. 4) are the sources that exhibit significant IDV. There are 22 sources (19 per cent of the total sample) that show modulation indices larger than 3σ at any frequency (8.6, 4.8 and 2.4 GHz) during either the May or August observing sessions. They are listed in Table 6.

In Table 6 there are 43 entries with $\mu > 3\sigma$ typed in bold. If these were purely random events, rather than any real effect, one would expect to see 4 sources showing two entries with $\mu > 3\sigma$, and no sources with three or more entries. Yet there are six sources with two entries, and six sources with three entries, and one source, PKS 1519−273, with four entries. Such a high incidence of multiple entries suggests that the results presented in Table 6 represent a real effect.

Out of these 22 IDVs, 10 (45 per cent) have a peaked spectrum, and 8 (36 per cent) have an inverted spectrum. The highest incidence of IDV occurs for inverted spectrum sources (39 per cent of all inverted-spectrum sources in the sample), followed by peaked-spectrum sources (24 per cent) and decreasing-spectrum sources (9 per cent).

4.4 Long-term variability (≤3 months)

The distribution of the fractional difference, F_ν, in the average flux density between 1994 May and August observations,

$$F_\nu = 2\frac{\bar{S}_\nu^{\rm May} - \bar{S}_\nu^{\rm Aug}}{\bar{S}_\nu^{\rm May} + \bar{S}_\nu^{\rm Aug}}, \qquad (2)$$

is shown in Fig. 5. The measurement errors of the fractional difference are estimated from the rms of the flux density measurement distributions. The 3σ level is less than 4 per cent for each frequency. We find that 40 per cent of sources vary by more than 4 per cent at 4.8 and 2.4 GHz. The number of sources variable on monthly time-scales becomes larger with increasing frequency.

A substantial fraction of IDV sources are also long-term variable (80 per cent at 8.6 GHz, 75 per cent at 4.8 GHz and 73 per cent at 2.4 GHz). This characteristic may prove useful in future searches for IDV sources.

Out of the 22 IDV sources, only six were found to show significant IDV in both observing sessions. The remainder of the sources (two-thirds) either have a shorter duty cycle than ∼3 months or their variability decreases below our 3σ inclusion limit. PKS 0405−385 is the most spectacular example of short-lived rapid variability (Kedziora-Chudczer et al. 1997). However, the other strong IDV sources (PKS 1034−293, PKS 1144−379 and PKS 1519−273) varied each time they were observed during the follow-ups of the Survey (Kedziora-Chudczer et al. 1998, 2000).

We also found that sources that show a difference in the shape of their total flux density spectrum between May and August sessions are twice as likely to show IDV as the sources without a significant spectral change. As seen from Fig. 5, these monthly spectral changes are not necessarily associated with the overall strong flux-density change at all frequencies.

4.5 Polarization variability

The polarization modulation index, μ_P, is defined as the rms of the polarized flux density normalized by the average polarized flux density. For the ATCA the instrumental polarization can be easily calibrated, therefore the main contribution to observed measurement errors comes from the antenna gain stability. The distribution of measured rms for three frequencies 8.6, 4.8 and 2.4 GHz is presented in Fig. 6. An estimate of the measurement error, $\sigma = 4$ mJy, was derived by finding the range of rms within which two-thirds of the sources are distributed around the peak of the distribution. Only 6 (8 per cent) of sources vary above 4σ at any frequency. These are PKS 0215+015, PKS 0537−441, PKS 0607−157, PKS 1144−379, PKS 1334−127 and PKS 1519−273. The most significant variability of polarized flux is seen for sources that were already identified as IDVs in the total flux density. The polarized flux density IDV of PKS 1334−127 is also independently found in VLBI data (Kochanev & Gabuzda 1998).

We also analysed the day-to-day polarization variability by self-calibrating each 24 h of data, which is equivalent to averaging the total flux density over this time (Table 7). Main advantage of such an approach is that the signal-to-noise ratio can be improved not only by averaging but also by removing the residual of the extended structure and confusion. The contribution of the extended flux density repeats over each 24 h provided the measurements are taken at similar hour angles each day and the confusing sources do not vary.

The distribution of the differences in polarized flux density between two days in each observing session is used to estimate the actual measurement error, $\sigma \sim 2.5$ mJy, which is only weakly dependent on frequency for the sources with polarization stronger than 15 mJy.

We find a number of sources with a total flux density IDV below 3σ but with a clearly variable polarization during a given observing session (Table 7), which indicates that the variable polarized component is only a small fraction of a quiescent total flux density of such sources.

The changes in polarization over three months are illustrated in a scatter plot (Fig. 7) of the averaged, polarized flux density data between 1994 May and August. The linear polarization appears to be more variable at high frequencies (4.8 and 8.6 GHz) similar to the monthly variations of the total flux density. Note that two sources (PKS 0646−306 and PKS 1610−771) show monthly changes in the polarized flux density without a significant change in their total flux density. We find that only three sources, PKS 0364−279, PKS 0537−441 and PKS 0607−157, show variable polarization on both the monthly and daily time-scales.

5 STATISTICAL PROPERTIES OF IDV

Various models of IDV phenomenon predict that the amplitudes and time-scales of variability can be related to the structure of the radio source, its properties or its position in relation to the plane of our Galaxy.

5.1 Dependence of modulation index on spectral index

Heeschen et al. (1987) showed that flat-spectrum sources are more likely to show intraday variability. We narrow that conclusion by finding that in our selection of flat-spectrum sources, those with inverted spectra over the observed range of frequencies, are more likely to show IDV than sources with other shapes of spectra. The flux densities of such sources are dominated by the most compact objects. This is an additional indicator that the rapid variability originates in the smallest source components.

Table 4. The average polarized flux densities ($\bar{P}$), the modulation indices of linear polarization ($\mu_{\bar{P}}$) and the average position angle of the polarized flux (ψ_2). The subscripts (1) and (2) correspond to measurements for 1994 May and August respectively at 8.6, 4.8, 2.4 and 1.4 GHz.

	8.6 GHz								4.8 GHz								2.4 GHz								1.4 GHz							
	94 May				94 August				94 May				94 August				94 May				94 August				94 May				94 August			
Source	N	$\bar{P}_1$	$\mu_{\bar{P}_1}$	ψ_1	N	$\bar{P}_2$	$\mu_{\bar{P}_2}$	ψ_2	N	$\bar{P}_1$	$\mu_{\bar{P}_1}$	ψ_1	N	$\bar{P}_2$	$\mu_{\bar{P}_2}$	ψ_2	N	$\bar{P}_1$	$\mu_{\bar{P}_1}$	ψ_1	N	$\bar{P}_2$	$\mu_{\bar{P}_2}$	ψ_2	N	$\bar{P}_1$	$\mu_{\bar{P}_1}$	ψ_1	N	$\bar{P}_2$	$\mu_{\bar{P}_2}$	ψ_2
name		mJy		deg		mJy		deg		mJy		deg		mJy		deg		mJy		deg		mJy		deg		mJy		deg		mJy		deg
0003−066	16	35	0.171	34.1	7	71	0.042	24.5	16	65	0.081	47.5	7	94	0.055	41.8																
0044−846	15	18	0.139	9.9					15	28	0.056	6.3																				
0104−408	17	66	0.098	−6.0	9	82	0.042	2.3	17	90	0.028	19.4	9	69	0.074	21.3	13	27	0.079	−74.7	9	35	0.056	−66.5								
0122−003									9	33	0.077	33.3	8	34	0.089	38.3																
0146+056	9	91	0.032	−64.2	7	93	0.017	−63.8	9	88	0.033	−66.7	7	78	0.027	−65.1	7	27	0.042	−69.7	7	22	0.065	−72.9								
0150−334	17	24	0.080	30.8	10	19	0.104	19.3	17	19	0.107	28.3	10	16	0.138	19.6									12	25	0.074	67.2	9	23	0.248	71.5
0202−172	9	18	0.123	−32.3	10	26	0.080	−42.6	9	81	0.053	−82.7	10	61	0.066	−81.4	11	57	0.028	−45.7	10	51	0.033	−44.7	11	39	0.070	−10.5	10	39	0.212	−13.3
0215+015									10	09	0.346	34.0	9	27	0.575	−35.5																
0220−349	13	26	0.089	−76.0	14	18	0.074	−71.8	13	25	0.065	−61.1	14	18	0.110	−55.6	16	16	0.145	−43.3	10	16	0.086	−43.9								
0252−549	17	39	0.039	−86.1																												
0302−623	12	34	0.214	−73.0	12	37	0.048	−68.4	12	45	0.074	−60.1	12	44	0.176	−51.8	18	46	0.083	−28.7	13	39	0.119	−25.2	18	38	0.160	48.3	13	44	0.157	51.6
0308−611	14	21	0.343	1.9	15	25	0.069	−3.6	14	25	0.146	5.2	15	26	0.227	10.6									11	44	0.080	−49.8	12	30	0.144	−52.8
0336−019	7	18	0.240	−37.1	8	22	0.150	−71.1																								
0346−279	9	30	0.085	19.0	11	19	0.089	19.7	9	39	0.068	29.7	11	24	0.105	26.5	7	28	0.153	41.7	11	28	0.068	44.3	7	27	0.115	−82.6	10	27	0.353	−78.4
0405−385	11	29	0.186	−22.8	76	22	0.071	−26.3	11	47	0.112	−24.5	76	35	0.068	−21.8	14	15	0.553	−12.8	77	22	0.087	−9.4								
0420−014	6	68	0.079	−69.1	11	74	0.030	−67.1	6	83	0.045	−75.3	11	76	0.059	−74.1	6	43	0.154	79.3	15	59	0.141	80.6	6	24	0.224	59.0	14	28	0.318	44.6
0426−380	15	21	0.290	−58.1	22	94	0.016	64.6																								
0440−003					11	29	0.059	40.6					11	54	0.069	65.6					11	18	0.132	−65.0					15	13	0.618	35.7
0450−469									15	21	0.139	18.3	21	19	0.066	23.1	11	30	0.064	32.2	24	26	0.086	35.7								
0454−810	16	55	0.110	4.9	17	44	0.138	11.1	16	41	0.139	14.8	17	34	0.154	−2.6									13	17	0.221	31.5	17	39	0.260	42.8
0457+024	7	29	0.126	17.3	12	33	0.070	19.6																								
0502+049	6	36	0.051	−38.8	9	40	0.052	−38.7	6	56	0.028	−32.7	9	52	0.032	−29.8									10	25	0.160	3.4	8	32	0.289	11.1
0537−441	12	42	0.501	−53.9	35	135	0.034	−82.7																								
0607−157	10	37	0.246	10.8	11	93	0.078	−10.9	10	17	0.358	−29.4	12	26	0.604	−46.3	8	58	0.091	29.7	11	58	0.075	29.7	8	48	0.106	−33.3	10	57	0.216	−31.6
0642−349	16	23	0.083	24.0	11	21	0.060	25.0	16	14	0.190	−9.5	11	17	0.158	−9.2																
0646−306	11	32	0.038	−31.6	16	24	0.103	−33.4	11	48	0.034	−24.7	16	34	0.104	−23.6	13	19	0.067	8.9	11	14	0.149	16.6								
0727−115	13	44	0.269	−19.5	12	56	0.077	77.5	13	66	0.100	−64.7	12	25	0.411	30.7	10	50	0.104	77.1	14	69	0.100	−77.6	10	59	0.142	−75.7	13	75	0.113	−71.0
0736+017	9	55	0.037	35.4	13	72	0.018	28.9	9	79	0.028	38.5	13	81	0.018	40.6	8	100	0.034	63.5	10	103	0.025	62.7	8	119	0.049	−83.0	10	129	0.082	−83.8
0808+019									9	19	0.227	−4.9	12	11	0.402	−8.2	13	22	0.247	−11.4	13	10	0.449	11.3								
0829+046	11	25	0.112	20.0	11	20	0.103	23.1	11	18	0.061	−11.0	11	14	0.150	−14.8	8	54	0.028	−4.0	12	48	0.056	−1.6	8	47	0.060	25.7	12	43	0.197	32.1
0834−201	10	15	0.261	26.8	12	16	0.085	−18.1									14	20	0.586	59.7	13	14	0.171	62.5								
0837+035	9	22	0.057	19.6	11	23	0.050	21.3	9	38	0.038	25.5	11	33	0.064	25.6	8	21	0.104	58.6	10	18	0.110	60.0								
1021−006	9	17	0.118	−32.6	7	17	0.045	−31.2	9	19	0.126	−20.1	7	17	0.100	−20.8																
1034−293	11	23	0.259	25.2	10	51	0.145	2.8	11	37	0.199	14.5	10	32	0.274	−2.3																
1048−313									15	21	0.101	−72.9	10	23	0.054	−73.5	11	20	0.124	−41.1	9	29	0.066	−43.3	11	16	0.167	43.2	9	35	0.142	46.9
1057−797	11	13	0.442	43.0	15	34	0.094	81.6									14	19	0.107	−76.1	19	23	0.155	−61.8	14	8	0.410	61.9	17	25	0.372	55.3
1115−122	11	18	0.113	−16.3	9	12	0.147	−4.7	11	26	0.072	8.5	9	22	0.087	13.3	9	41	0.024	−12.9	9	34	0.086	−16.4								
1127−145	9	91	0.086	−17.7	9	108	10.09	−17.8	9	152	0.056	−20.1	9	132	0.097	−20.0	13	84	0.069	20.9	11	76	0.076	21.5	12	43	0.057	81.7	9	229	0.143	80.3
1144−379	12	50	0.244	32.4	9	86	0.272	47.7	12	75	0.059	33.8	9	62	0.146	60.8																
1148−001	9	44	0.046	−52.2	9	47	0.013	−54.5	9	77	0.019	−49.0	9	67	0.049	−5	11	117	0.023	−43.3	8	104	0.026	−43.0	11	143	0.050	−37.4	8	136	0.097	−40.1

Table 4 – *continued*

Source name	8.6 GHz 94 May N	$\bar{P}_1$ mJy	$\mu_{\bar{P}_1}$	ψ_1 deg	8.6 GHz 94 August N	$\bar{P}_2$ mJy	$\mu_{\bar{P}_2}$	ψ_2 deg	4.8 GHz 94 May N	$\bar{P}_1$ mJy	$\mu_{\bar{P}_1}$	ψ_1 deg	4.8 GHz 94 August N	$\bar{P}_2$ mJy	$\mu_{\bar{P}_2}$	ψ_2 deg	2.4 GHz 94 May N	$\bar{P}_1$ mJy	$\mu_{\bar{P}_1}$	ψ_1 deg	2.4 GHz 94 August N	$\bar{P}_2$ mJy	$\mu_{\bar{P}_2}$	ψ_2 deg	1.4 GHz 94 May N	$\bar{P}_1$ mJy	$\mu_{\bar{P}_1}$	ψ_1 deg	1.4 GHz 94 August N	$\bar{P}_2$ mJy	$\mu_{\bar{P}_2}$	ψ_2 deg
1243−072	14	21	0.124	27.2	6	13	0.068	16.1	14	26	0.109	20.6	6	20	0.174	18.9	11	23	0.076	36.5	7	19	0.094	34.6	11	27	0.096	66.4	7	19	0.705	65.1
1255−316	15	46	0.085	−54.5	8	44	0.036	−54.2	15	48	0.051	−58.9	8	41	0.054	−59.7									18	66	0.034	−20.3	11	54	0.168	−20.1
1256−220	16	15	0.146	48.1	7	16	0.084	69.0									11	20	0.121	16.6	7	18	0.047	17.6	11	23	0.110	−30.3	7	28	0.501	−30.9
1334−127	10	119	0.164	78.6	7	163	0.102	−75.4																								
1351−018	14	18	0.168	−40.2	6	14	0.097	−45.0																								
1406−076	11	25	0.085	−44.6	7	18	0.078	−63.6	11	18	0.160	−45.2	7	15	0.190	−54.6																
1435−218	14	14	0.158	−9.9	8	21	0.079	−12.3	14	23	0.071	−5.0	8	24	0.090	−6.8																
1443−162	12	38	0.038	−51.3	7	31	0.041	−50.3	12	36	0.065	−59.2	7	25	0.072	−58.6																
1504−166	12	61	0.088	33.8	7	70	0.039	29.3	12	42	0.128	19.7	7	41	0.194	17.1																
1519−273	15	45	0.195	−30.2	7	18	0.287	−20.0	15	62	0.319	−24.0	7	26	0.331	−35.2	10	24	0.305	17.5	8	28	0.085	41.4	10	07	0.597	46.2	8	21	0.540	−33.9
1610−771	16	106	0.077	−68.5	13	135	0.015	−67.2	16	122	0.054	−71.7	13	104	0.088	−68.1																
1622−297	11	100	0.045	16.4	10	108	0.042	12.8	11	119	0.015	9.9	10	121	0.030	9.0	10	165	0.033	−26.3	9	142	0.020	−25.3								
1718−649									14	12	0.240	−10.7	9	17	0.350	−20.1	17	26	0.448	36.2	9	11	0.384	−15.9	18	11	0.221	7.9	9	20	0.684	10.9
1741−038	11	29	0.252	69.0	6	25	0.263	−76.9	11	21	0.168	52.5	6	31	0.131	60.3	13	22	0.146	66.4	6	21	0.075	79.2	13	17	0.275	−73.1	6	16	0.354	−38.9
1815−553	14	42	0.059	81.5	8	18	0.040	80.1	14	40	0.052	−84.1	8	15	0.352	−36.6																
1921−293	12	486	0.096	−31.5	11	515	0.056	−67.1	12	567	0.076	17.7	11	249	0.103	82.3	9	604	0.022	18.9	10	295	0.085	22.8	9	359	0.074	−21.9	8	462	0.034	−25.8
1925−610	8	37	0.067	64.2	7	42	0.031	69.6	12	35	0.076	58.7	7	29	0.105	61.2	21	30	0.076	77.6	7	24	0.059	12.4	21	32	0.075	−13.3	7	34	0.193	−7.2
1937−101									8	19	0.116	−22.6	6	18	0.142	−28.5									12	15	0.413	64.3	7	14	0.352	68.1
1958−179	9	26	0.085	84.3	6	21	0.053	79.9	9	39	0.114	69.0	6	28	0.059	78.0	8	44	0.060	32.5	6	36	0.035	43.2								
2058−297	8	16	0.111	1.2	8	16	0.101	−85.9	8	20	0.053	43.2	8	18	0.076	83.0	9	19	0.064	−73.1	8	18	0.065	−76.0	9	18	0.076	65.4	8	20	0.384	46.9
2106−413	9	58	0.100	66.8	11	65	0.026	68.0	9	41	0.067	44.8	11	22	0.218	51.6	10	51	0.045	69.6	7	47	0.057	72.9	10	61	0.072	81.4	7	54	0.197	35.0
2121+053	11	36	0.070	59.3	5	17	0.170	76.1	11	45	0.073	63.7	5	25	0.190	58.7	9	35	0.133	65.4	5	31	0.050	51.5	9	42	0.107	68.4	5	25	0.433	55.8
2128−123	10	11	0.572	18.1	8	18	0.123	−12.6	10	21	0.222	−61.9	8	24	0.188	−63.6	9	17	0.131	−44.4	7	14	0.147	−46.4	9	32	0.068	−52.9	7	32	0.229	−5
2134+004					7	100	0.082	−88.2					7	47	0.272	40.5					7	33	0.244	33.9					7	14	0.784	15.4
2142−758	13	15	0.124	73.0	12	20	0.069	72.4	13	16	0.124	70.6	12	18	0.139	78.4																
2149−307	12	73	0.025	44.1	6	79	0.030	41.0	12	83	0.049	57.1	6	73	0.019	55.4	17	38	0.077	81.3	6	33	0.079	83.9	17	28	0.166	65.8	6	28	0.242	63.0
2155−304									21	18	0.237	−24.5	6	16	0.085	−26.3	20	17	0.236	−20.6	9	14	0.337	−26.9								
2243−123	14	52	0.080	21.1	7	48	0.048	15.9	14	14	0.229	36.6	7	22	0.277	24.8	11	31	0.099	−15.6	7	24	0.180	−17.5	11	36	0.105	−39.1	7	36	0.204	−41.4
2312−319	9	14	0.096	−83.8	8	17	0.056	−82.7	9	24	0.090	−85.1	8	23	0.081	−82.6	12	31	0.077	−74.1	7	28	0.059	−72.3								
2326−477	16	47	0.114	−23.3	8	52	0.025	−31.3	16	89	0.032	−3	8	81	0.063	−29.1	13	128	0.017	−19.1	9	111	0.039	−19.2	13	137	0.040	−61.8	8	126	0.108	1.0
2329−384	10	25	0.077	71.7					10	28	0.051	87.5																				
2332−017	11	21	0.167	−24.9	7	17	0.103	−22.4	11	32	0.084	−33.5	7	23	0.060	−31.9																
2345−167	11	60	0.117	16.2	7	48	0.031	3.3	11	55	0.132	9.7	7	43	0.204	13.7									13	49	0.165	−1.0	7	46	94	9.4
2355−534	14	31	0.154	−4.2	8	25	0.073	−15.4	14	48	0.126	−10.6	8	49	0.107	−13.4																

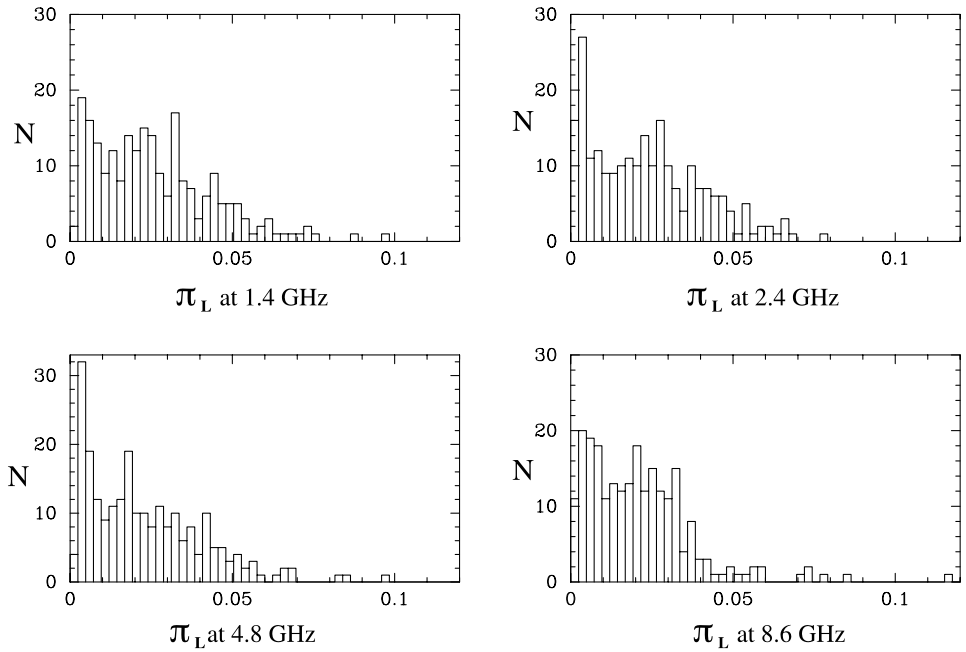

Figure 1. Distribution of the fractional linear polarization averaged over a duration of each observing session (1994 May and August combined) for all sources in the sample.

The modulation index as a function of the four spectral indices (Table 5) was used to search for a correlation between high modulation index and inverted spectra. We calculated the mean spectral index for all non-variable sources ($\mu < 3\sigma$) at a given frequency, and compared it with the mean spectral index of IDVs ($\mu \geq 3\sigma$) for $\alpha_{4.8}^{8.6}$, $\alpha_{2.4}^{4.8}$ and $\alpha_{1.4}^{8.6}$. The mean spectral index differences for these two groups of sources are -0.12, -0.06 and -0.05 respectively. The only significant difference occurred for high frequency spectral index, $\alpha_{4.8}^{8.6}$.

The lack of strong correlation between the spectral index and modulation indices suggests that the IDV strength is not a simple function of the source size.

5.2 Intraday variability as a function of Galactic coordinates

The interstellar scintillation (ISS) model predicts different amplitudes and time-scales of IDV depending on the source position with respect to the plane of our Galaxy. The detailed properties of variability depend on the strength of the scattering in the Galactic medium as well as a size of the scintillating source (see e.g. Narayan 1992; Walker 1998). The scattering strength is related to the amount of turbulence in the Galactic medium and it is derived mostly from observations of the scattering measure in pulsars. A model of the Galactic interstellar medium was developed by Taylor & Cordes (1993) from pulsar observations. Applying this model to the theory of ISS (Walker 1998), the following predictions can be made.

(i) Variability of a point source is strongest and most rapid at *the transition frequency*, which corresponds to a scattering strength equal to unity. The transition frequency increases towards the Galactic plane and ranges from a few GHz near the Galactic poles to a few tens of GHz at the Galactic plane.

(ii) The time-scale of variability at the transition frequency is of the order of a few hours and does not depend strongly on the Galactic position.

(iii) The angular size of a variable source has to be comparable to the size of the first Fresnel zone, θ_F, at the transition frequency. The predicted source sizes are of the order of μarcsec. Sources larger than θ_F scintillate with decreased amplitude and longer time-scale.

The sample of IDV sources found during the ATCA IDV Survey provides an opportunity to test the above model predictions. The Galactic positions of IDV sources from Table 6 at one of the three frequencies 8.6, 4.8 and 2.4 GHz (Fig. 8a) are compared with the Galactic distribution of all sources in the Survey (Fig. 8b).

The ISS model predicts that the maximum variability for a source with $\theta \leq \theta_F$ should occur at the transition frequency, which in turn is a strong function of the Galactic latitude. From Fig. 8a it is quite clear that the distribution of variability maxima, which are marked with different symbols for different frequencies, does not follow this prediction. The maxima of variability at different frequencies appear randomly distributed in otherwise non-random region where IDV prevails.

The reasons that may contribute to the lack of clear dependence of the frequency of strongest IDV on the Galactic latitude are the deficiencies of the ISM model, the source size effects and the uncertainties in measurement of modulation indices. The Taylor & Cordes model is most accurate at latitudes close to Galactic plane, where the number of pulsars is largest. An excess of IDV sources in the swathe between 210° and 250° of Galactic longitude reaching towards high Galactic latitudes may correspond to real features of the ISM, which are not described well by the pulsar-based model.

The modulation index and time-scale of variability depends on the size of the source. In Fig. 8 the maximum modulation index is assumed to occur at the transition frequency. However if the intrinsic size of the radio source increases with decreasing frequency as $\theta_S \propto \nu^{-1}$ (Kellermann & Owen 1988), the peak of variability may occur at lower frequency than expected for the point source at a given latitude. This may explain the presence of low-frequency 'μ-peakers' at low Galactic latitudes. The sources, which show the highest μ at latitudes higher than expected from

Table 5. The average spectral indices for two observing sessions: 1994 May and August.

PKS Source name	1994 May $\alpha_{4.8}^{8.6}$	$\alpha_{2.4}^{4.8}$	$\alpha_{1.4}^{2.4}$	$\alpha_{1.4}^{8.6}$	1994 August $\alpha_{4.8}^{8.6}$	$\alpha_{2.4}^{4.8}$	$\alpha_{1.4}^{2.4}$	$\alpha_{1.4}^{8.6}$
0003−066	−0.06	0.24	0.34	0.17	−0.13	0.24	0.43	0.18
0013−005	−0.33	−0.14	0.09	−0.13	−0.41	−0.10	0.12	−0.14
0023−263	−0.93	−0.74	−0.66	−0.78	−0.99	−0.73	−0.68	−0.80
0044−846	−0.27	−0.10	−0.15	−0.17				
0048−427	0.24	0.36	0.33	0.31	0.14	0.41	0.39	0.32
0056−572	−0.20	0.01	0.10	−0.03	−0.23	−0.01	0.09	−0.05
0104−408	0.88	0.76	0.46	0.71	0.89	0.94	0.30	0.73
0122−003	−0.09	0.05	0.02	0.00	−0.08	0.03	0.10	0.01
0131−522	0.24	0.12	−0.39	0.01				
0138−097	−0.08	0.16	0.09	0.06	−0.03	0.16	0.25	0.12
0142−278	−0.09	0.09	−0.17	−0.04	−0.29	0.02	−0.06	−0.10
0146+056	−0.09	0.30	0.50	0.24	−0.11	0.30	0.50	0.23
0150−334	−0.28	−0.08	−0.03	−0.13	−0.36	−0.12	−0.05	−0.18
0202−172	0.02	0.21	0.08	0.11	−0.07	0.22	0.10	0.09
0208−512	0.03	−0.09	−0.07	−0.04				
0214−522	−0.70	−0.48	−0.36	−0.52	−0.74	−0.49	−0.36	−0.53
0215+015	0.40	0.04	−0.16	0.09	0.35	0.28	0.10	0.25
0220−349	−0.07	0.17	0.12	0.08	−0.09	0.21	0.20	0.12
0252−549	0.06	0.09	−0.02	0.05				
0302−623	−0.17	−0.03	−0.03	−0.07	−0.19	0.00	0.13	−0.02
0308−611	0.34	0.46	0.18	0.34	0.28	0.46	0.23	0.33
0334−546	−0.50	0.07	0.50	0.01	−0.53	0.05	0.48	0.00
0336−019	−0.04	0.11	0.21	0.09	−0.16	0.07	0.10	0.01
0346−279	0.05	0.21	0.17	0.14	0.11	0.17	0.18	0.15
0355−483	−0.43	0.17	0.22	−0.01				
0405−385	0.08	0.29	0.38	0.25	0.08	0.24	0.33	0.22
0420−014	−0.13	0.04	0.30	0.07	−0.13	−0.14	−0.13	−0.13
0422+004	0.18	0.19	−0.05	0.11				
0426−380	0.37	0.56	0.37	0.44	0.14	0.42	0.46	0.34
0434−188	−0.15	0.25	0.61	0.23	−0.15	0.29	0.64	0.26
0437−454	−0.06	−0.05	−0.13	−0.08	0.09	0.00	0.12	0.07
0440−003					−0.19	0.02	0.20	0.01
0450−469	−0.31	−0.16	−0.16	−0.21	−0.23	−0.02	0.01	−0.08
0454−463	−0.28	−0.26	−0.50	−0.34				
0454−810	0.15	0.15	0.35	0.21	0.21	0.39	0.30	0.31
0457+024	−0.50	−0.19	0.06	−0.22	−0.55	−0.18	0.07	−0.22
0502+049	−0.40	−0.22	0.09	−0.19	−0.12	−0.21	0.08	−0.09
0522−611	−0.02	−0.02	−0.17	−0.06	−0.12	−0.08	−0.17	−0.12
0528−250	−0.52	−0.43	0.05	−0.32	−0.54	−0.38	0.14	−0.28
0537−286	−0.67	−0.42	−0.09	−0.40	−0.59	−0.42	0.02	−0.35
0537−441	0.32	0.47	0.31	0.37	0.34	0.28	0.51	0.37
0607−157	0.39	0.41	−0.03	0.27	0.55	0.56	0.13	0.43
0642−349	−0.30	0.20	0.20	0.04	−0.33	0.18	0.23	0.03
0646−306	−0.03	0.42	0.14	0.19	−0.10	0.20	0.33	0.14
0648−165	0.06	0.02	−0.21	−0.04	0.13	0.03	−0.28	−0.03
0727−115	−0.08	0.36	0.36	0.22	−0.06	0.23	0.44	0.20
0728−320	−0.54	−0.20	0.12	−0.21	−0.70	−0.44	0.26	−0.31
0733−174	−0.62	−0.46	−0.11	−0.40	−0.60	−0.42	−0.18	−0.41
0736+017	−0.12	−0.11	−0.24	−0.15	−0.30	−0.43	−0.37	−0.37
0808+019	0.09	0.28	0.17	0.19	−0.06	0.08	0.00	0.01
0829+046	0.09	0.17	0.05	0.11	0.20	0.16	0.09	0.15
0834−201	0.34	0.17	−0.28	0.09	0.33	0.11	−0.22	0.08
0837+035	−0.16	0.08	0.16	0.03	−0.14	0.04	0.14	0.01
1021−006	−0.68	−0.39	0.04	−0.35	−0.67	−0.44	0.03	−0.37
1034−293	0.73	0.82	−0.07	0.52	0.45	0.29	0.42	0.38
1036−154	0.10	0.03	−0.10	0.01	0.08	0.00	−0.03	0.02
1048−313	−0.30	−0.06	0.12	−0.08	−0.30	−0.15	0.04	−0.14
1057−797	0.01	0.48	0.71	0.40	0.05	0.60	0.45	0.38

Table 5 – *continued*

PKS Source name	1994 May $\alpha_{4.8}^{8.6}$	$\alpha_{2.4}^{4.8}$	$\alpha_{1.4}^{2.4}$	$\alpha_{1.4}^{8.6}$	1994 August $\alpha_{4.8}^{8.6}$	$\alpha_{2.4}^{4.8}$	$\alpha_{1.4}^{2.4}$	$\alpha_{1.4}^{8.6}$
1105−680	−0.24	0.39	0.93	0.35	−0.33	0.28	0.91	0.27
1115−122	0.08	0.08	−0.17	0.00	0.03	−0.07	−0.15	−0.06
1127−145	−0.39	−0.30	−0.26	−0.31	−0.41	−0.33	−0.26	−0.33
1143−245	−0.56	−0.23	0.20	−0.21	−0.53	−0.24	0.28	−0.18
1144−379	−0.10	0.22	−0.20	−0.01	0.09	0.11	0.36	0.18
1148−001	−0.56	−0.41	−0.37	−0.45	−0.56	−0.47	−0.34	−0.46
1148−671	−0.65	−0.15	0.68	−0.06	−0.68	−0.10	0.86	0.00
1243−072	0.37	0.46	0.27	0.38	0.36	0.38	0.33	0.36
1253−055	0.32	0.29	0.15	0.26	0.29	0.26	0.41	0.31
1255−316	−0.09	0.29	0.23	0.15	−0.10	0.38	0.37	0.22
1256−220	0.25	−0.11	−0.22	−0.03	0.49	−0.04	−0.26	0.06
1334−127	0.29	0.56	0.44	0.44	0.33	0.35	0.52	0.39
1351−018	−0.24	0.25	0.34	0.12	−0.22	0.20	0.37	0.12
1354−152	−0.16	0.34	0.35	0.18	−0.05	0.20	0.39	0.18
1402−012	−0.61	−0.36	−0.26	−0.41	−0.59	−0.38	−0.19	−0.39
1406−076	0.49	0.50	0.00	0.34	0.37	0.45	0.09	0.32
1435−218	−0.17	−0.15	−0.12	−0.15	−0.07	−0.14	−0.01	−0.08
1443−162	0.04	0.12	−0.20	0.00	−0.03	0.06	−0.10	−0.02
1502+036	0.07	0.10	0.22	0.13	0.12	0.64	0.48	0.42
1504−166	−0.11	−0.02	−0.05	−0.06	−0.10	0.02	−0.04	−0.04
1519−273	−0.03	0.40	0.20	0.20	0.04	0.43	0.62	0.36
1535+004	−0.46	−0.20	−0.10	−0.25	−0.45	−0.21	−0.03	−0.23
1540−828	−0.25	−0.14	−0.34	−0.23	−0.29	−0.11	−0.27	−0.21
1549−790	−0.63	−0.21	−0.14	−0.33				
1555−140	−0.60	−0.14	0.81	0.00	−0.61	−0.18	0.85	−0.01
1556−245	−0.59	−0.53	−0.47	−0.53	−0.54	−0.47	1.42	0.07
1610−771	−0.01	−0.02	−0.21	−0.07	0.01	0.01	−0.12	−0.03
1619−680	−0.53	−0.08	0.38	−0.09	−0.56	−0.01	0.36	−0.08
1622−297	−0.05	0.12	0.06	0.05	−0.04	0.10	−0.18	−0.03
1718−649	−0.35	0.09	0.32	0.02	−0.40	0.08	0.34	0.00
1741−038	0.41	0.42	0.35	0.40	0.56	0.49	0.51	0.52
1758−651	0.10	0.11	−0.24	0.00	0.10	0.13	−0.22	0.01
1815−553	−0.10	0.27	0.32	0.16	−0.15	−0.06	0.01	−0.06
1921−293	0.33	0.60	0.25	0.41	0.25	0.42	0.25	0.32
1925−610	0.03	0.37	0.11	0.19	−0.08	0.31	0.15	0.14
1937−101	−0.37	−0.23	−0.01	−0.21	−0.40	−0.16	0.12	−0.15
1958−179	−0.34	−0.23	−0.12	−0.23	−0.16	−0.29	−0.32	−0.26
2016−615	−0.69	−0.51	−0.49	−0.56				
2052−474	−0.23	−0.10	−0.17	−0.16	−0.31	−0.12	0.08	−0.12
2058−297	−0.25	−0.03	0.54	0.07	−0.20	0.04	0.10	−0.02
2106−413	0.23	0.25	0.09	0.20	0.10	0.31	0.11	0.18
2109−811					−0.03	0.18	0.27	0.14
2121+053	−0.33	−0.10	0.01	−0.14	−0.27	−0.02	0.14	−0.05
2126−158	−0.35	0.40	0.89	0.31	−0.36	0.38	0.86	0.28
2128−123	0.17	0.30	0.32	0.27	0.25	0.34	0.33	0.31
2134+004					−0.23	0.42	1.20	0.45
2142−758	−0.36	−0.27	−0.27	−0.30	−0.37	−0.25	−0.21	−0.28
2146−783	−0.51	0.23	0.68	0.13	−0.53	0.21	0.61	0.09
2149−307	−0.22	0.29	0.33	0.14	−0.34	0.20	0.33	0.06
2155−304	−0.03	0.10	0.07	0.05	−0.04	0.08	−0.03	0.01
2243−123	0.05	0.26	0.17	0.17	0.05	0.24	0.14	0.15
2245−328	0.07	−0.16	−0.41	−0.16				
2312−319	−0.46	−0.35	−0.28	−0.36	−0.50	−0.38	−0.24	−0.38
2320−035	−0.09	−0.02	−0.09	−0.06	−0.16	0.01	−0.02	−0.05
2326−477	−0.07	−0.29	−0.40	−0.25	−0.09	−0.29	−0.36	−0.25
2329−384	−0.48	−0.01	0.32	−0.06				
2332−017	−0.25	−0.11	−0.02	−0.13	−0.30	−0.13	0.07	−0.12

Table 5 – *continued*

PKS Source name	1994 May $\alpha_{4.8}^{8.6}$	$\alpha_{2.4}^{4.8}$	$\alpha_{1.4}^{2.4}$	$\alpha_{1.4}^{8.6}$	1994 August $\alpha_{4.8}^{8.6}$	$\alpha_{2.4}^{4.8}$	$\alpha_{1.4}^{2.4}$	$\alpha_{1.4}^{8.6}$
2333−528	−0.29	−0.16	−0.19	−0.21	−0.33	−0.16	0.05	0.18
2345−167	−0.16	0.29	0.01	0.06	−0.07	0.20	0.18	0.11
2355−534	−0.25	0.18	0.04	0.00	−0.14	0.04	0.06	−0.01

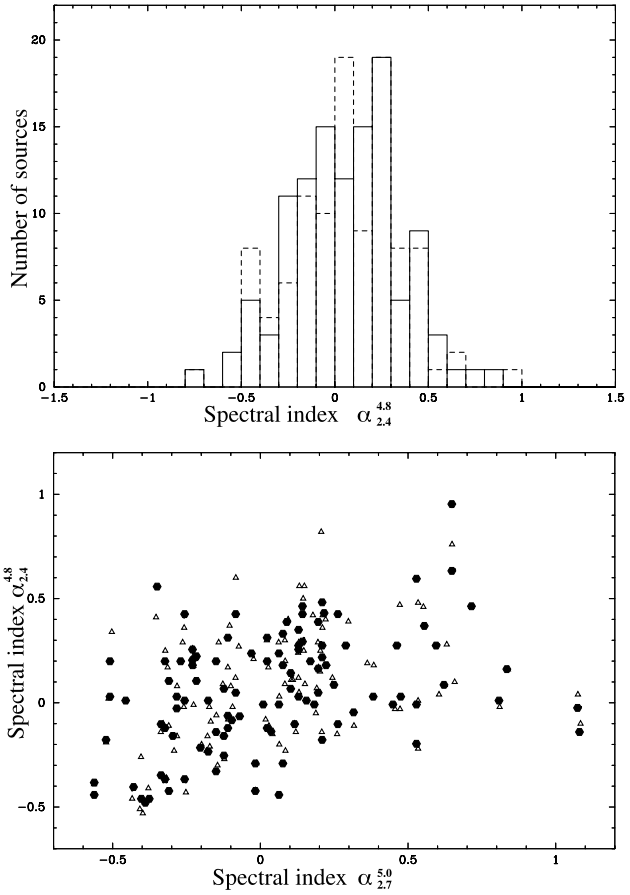

Figure 2. Upper panel: the number distribution of the Survey spectral indices $\alpha_{2.4}^{4.8}$ of all compact sources for 1994 May (full line) and August (dashed line). Lower panel: the scatter plot of Parkes spectral indices $\alpha_{2.7}^{5.0}$ versus spectral indices $\alpha_{2.4}^{4.8}$ of all sources for 1994 May (hexagons) and August (triangles).

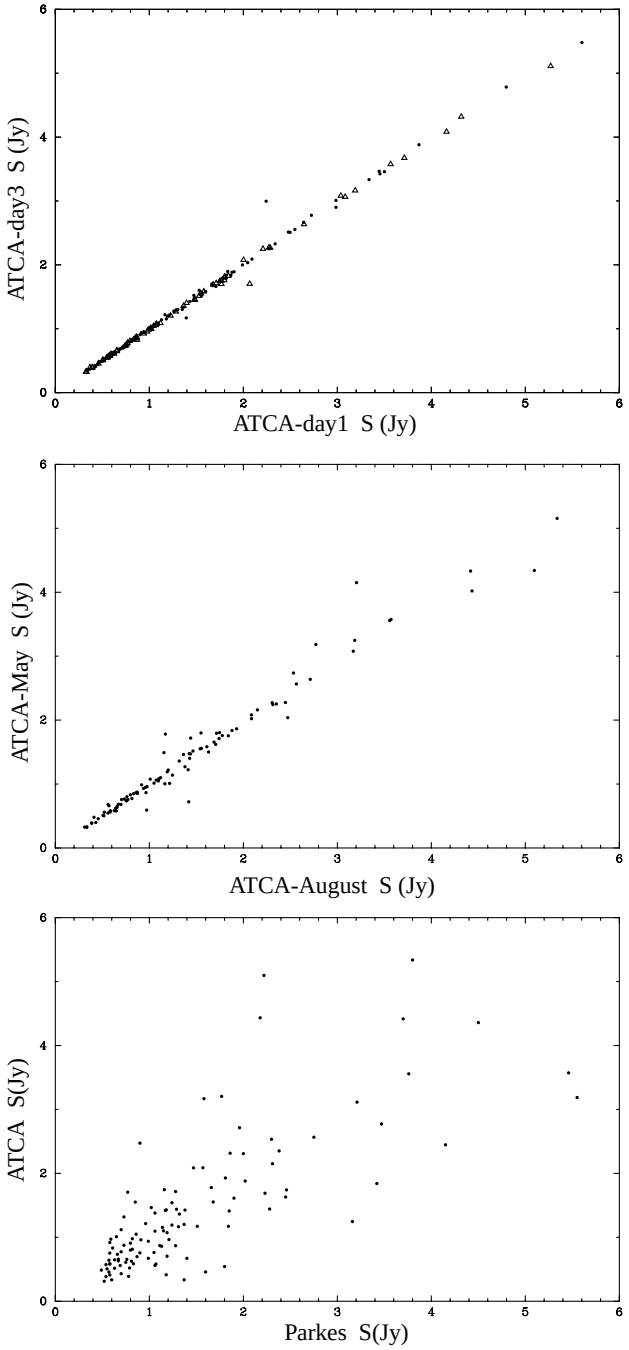

Figure 3. Comparison of flux densities at 4.8 GHz for progressively longer time separations. Top: the measurements taken one day apart with the ATCA; dots – May data, triangles – August data. Middle: the average flux densities measured 3 months apart with the ATCA. Bottom: the measurements with ATCA in 1994 May plotted against flux densities listed in the Parkes catalogue.

the Taylor & Cordes ISM model, may be explained if their compact, variable components become self-absorbed at low frequencies.

In addition, the time-scale of 96 h may not be sufficient to sample over many 'scintles', especially at lower frequencies. Therefore our measured modulation indices are in many cases only lower limits of the typical modulation indices of the scintillating sources.

6 DISCUSSION

6.1 Properties of IDV sources

The properties of IDV observed in any Survey may depend on the choice of the parent sample. Although the flat-spectrum flux

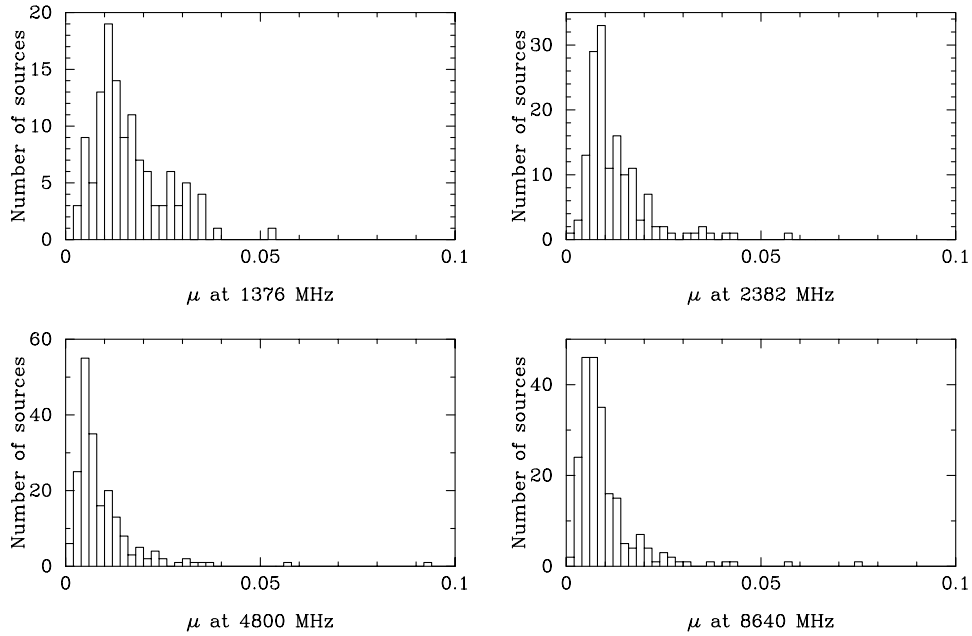

Figure 4. The combined distribution of modulation indices over two observing sessions, 1994 May and August, for all frequencies.

Table 6. The list of sources that show modulation indices exceeding 3σ for any of the frequencies, 2.4, 4.8 and 8.6 GHz, in any of the two observing sessions: 1994 May (μ_M) and August (μ_A). Entries in bold are those specifically $> 3\sigma$.

Source name	8.6 GHz		4.8 GHz		2.4 GHz	
	μ_M	μ_A	μ_M	μ_A	μ_M	μ_A
0104−408	0.011	0.003	0.013	0.004	**0.044**	0.007
0346−279	0.009	0.007	**0.030**	0.015	0.016	0.022
0405−385	**0.043**	0.003	**0.056**	0.007	**0.056**	0.011
0422+004	0.018		**0.024**			
0437−454	**0.025**	0.009	0.016	0.014		
0440−003		**0.029**		0.011		0.018
0450−469	0.012	0.003	0.016	0.004	**0.034**	0.006
0502+049	0.005	**0.027**	0.018	0.011		
0528−250	**0.020**	0.009	0.014	0.005		
0607−157	0.012	0.005	0.013	**0.023**	0.013	**0.031**
0646−306	0.014	0.012	**0.024**	0.011	**0.037**	0.024
0728−320	**0.026**	0.011	**0.034**	0.007		
0808+019	0.014	**0.021**	0.011	**0.023**	**0.025**	0.022
1034−293	**0.057**	0.012	**0.092**	**0.113**		
1048−313	**0.026**	0.019	0.011	**0.025**	0.023	0.010
1144−379	**0.075**	0.017	**0.146**	**0.031**		
1256−220	0.012	**0.027**	0.014	**0.022**	0.009	0.007
1502+036	**0.020**	0.002	0.014	0.008		
1519−273	**0.029**	0.018	**0.037**	**0.023**	**0.040**	0.009
1556−245	0.015	**0.042**	**0.028**	**0.033**		
1622−297	**0.020**	**0.031**	0.011	0.014	0.021	0.016
2155−304	**0.024**	0.008	**0.021**	0.005	**0.034**	0.020

density-limited sample of sources used in our Survey was selected on the basis their radio compactness, without distinction based on the type of the object, the majority of the selected sources are blazars [i.e. flat-spectrum radio quasars (FSRQ) and radio selected BL Lac objects], which tend to be both compact and luminous (Urry & Padovani 1995). In order to show IDV the sources have to be compact regardless of which interpretation of IDV is preferred. The size of the source is dictated by causality arguments in case of intrinsic variability. Similarly the ISS effects are strongest for the very compact sources.

The IDV sources found in the ATCA Survey consist of six BL Lacs and 16 quasars. This is almost 50 per cent of the BL Lacs from the original sample, as compared with only 20 per cent of quasars. Notably the Survey sample contains seven radio sources identified as galaxies, none of which showed intraday variability.

Modulation indices derived for the IDV sources are typically less than 10 per cent. We found that only a small fraction of the sources (2.5 per cent) show occasional stronger variations. Variability appears to be quasiperiodic, which is evident from well-sampled light curves, such as that for PKS 0405−385 (Kedziora-Chudczer et al. 1997). The largest modulation indices are typically found at 4.8 and 2.4 GHz.

The present Survey was designed to explore time-scales between 2 h and ∼3 d. Characteristic time-scales were found to depend on the observed frequency. For the best-sampled lightcurves of a few IDV sources in our sample it is evident that the time-scale of variability decreases with frequency.

In present survey we find that most of the IDV sources are at relatively low redshifts. If we interpret IDV as a propagation effect, it should be more frequent for the more distant sources of the same size. For instance, ISS depends on the distance of the source only through its angular size. However the compact, scintillating components of a distant source have to be sufficiently bright in order to measure any flux density changes. The very compact components of the nearby sources can satisfy such a signal-to-noise ratio requirement more easily.

The following properties of IDV sources were identified at different wavelengths. A substantial number (40 per cent) of our IDV sources are known to be optically variable objects, which show high and variable optical polarization. Four of them (PKS 0422+004, PKS 0808+019, PKS 1144−379 and PKS 2155−304) are BL Lacs, the others (PKS 0440−003, PKS 0528−250, PKS 0607−157, PKS 0646−306 and PKS 1622−297) are quasars. Most of the IDVs in our sample are only weak sources of X-ray and γ-ray emission, which is a selection bias rather than a real effect. One of the more unusual sources in this respect is PKS 1622−297, which showed a strong γ-ray outburst when its energy increased ∼200 times within a few days (Mattox et al. 1997).

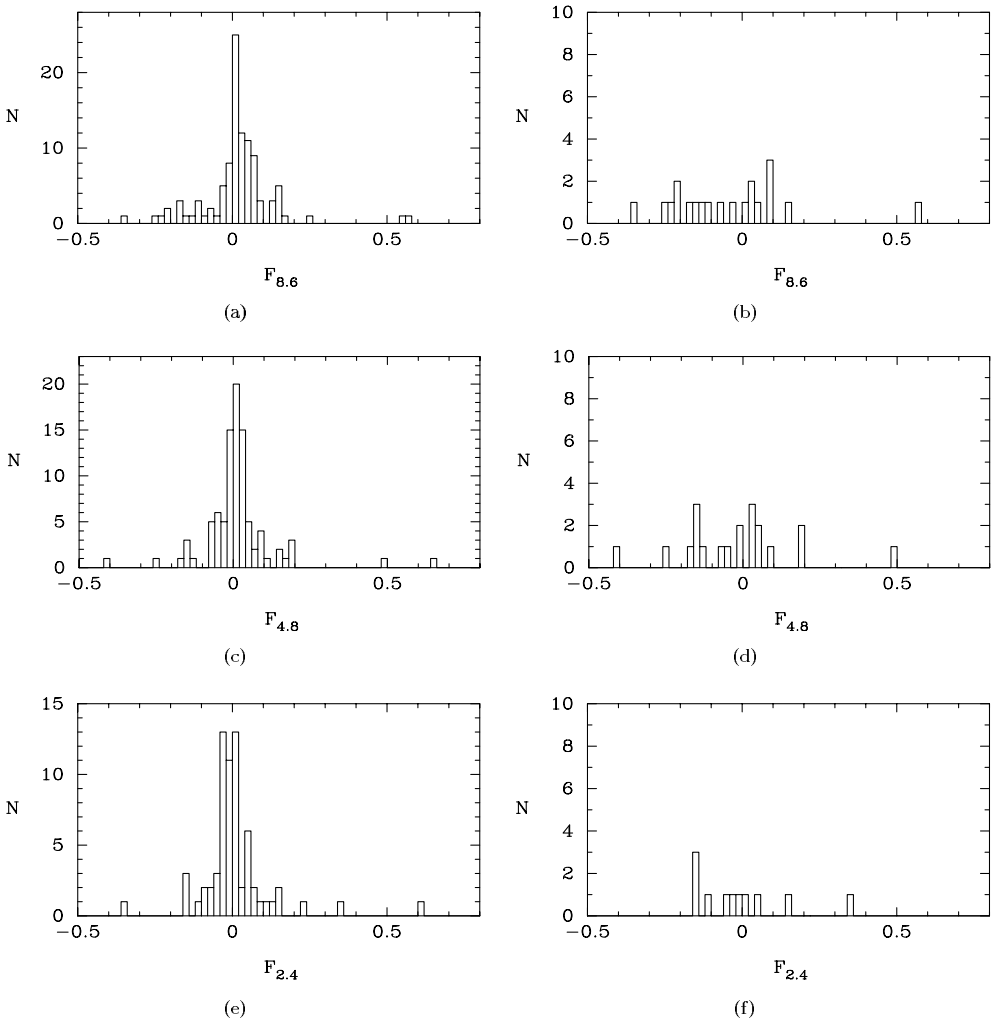

Figure 5. Distribution of the fractional difference in average flux density between two observing sessions: 1994 May and August. Left panels: the whole sample. Right panels: only IDV sources from Table 6 are included.

Table 7. The list of sources that have their day-to-day polarized flux densities differences larger than 3σ in any of the two observing sessions: 1994 May ($\Delta P_{\rm M}$) and August ($\Delta P_{\rm A}$).

Source name	8.6 GHz		4.8 GHz		2.4 GHz	
	$\Delta P_{\rm M}$	$\Delta P_{\rm A}$	$\Delta P_{\rm M}$	$\Delta P_{\rm A}$	$\Delta P_{\rm M}$	$\Delta P_{\rm A}$
0150−334	−0.006	**−0.009**	−0.002	0.005	−0.003	−0.004
0727−115	**0.009**		−0.006		**0.011**	
1334−127	0.000		**0.010**		0.001	
1504−166	0.002	0.003	−0.001	0.007	**0.010**	**0.011**
1622−297		0.003		**0.072**		**−0.085**
2106−413	0.004	**0.020**	0.001	0.000	−0.002	−0.001
2149−307		−0.001		0.003		**0.015**
2155−304		**0.024**		−0.005		**0.010**
2312−319		**−0.011**		**0.009**		**0.016**

PKS 2155−304 is an IDV source, which shows unusually strong X-ray emission. It is known to show rapid X-ray, optical and UV variability (Allen et al. 1993). This is the only source that was included in our Survey purely for its interesting properties (it violates the flux density limit in our selection criteria). Our IDV observations of PKS 2155−304 were used as a part of its multiwavelength monitoring campaign (Pesce et al. 1997). An important result of this monitoring is the lack of correlation between radio and higher energy flux density changes for this source.

However, the presence of correlation between optical and radio variability is claimed for another IDV source, S5 0716+714 (Quirrenbach et al. 1991). To resolve the question of correlated or otherwise variability of IDV sources at high and low energies, intensive multiwavelength monitoring of known IDV sources was undertaken recently.

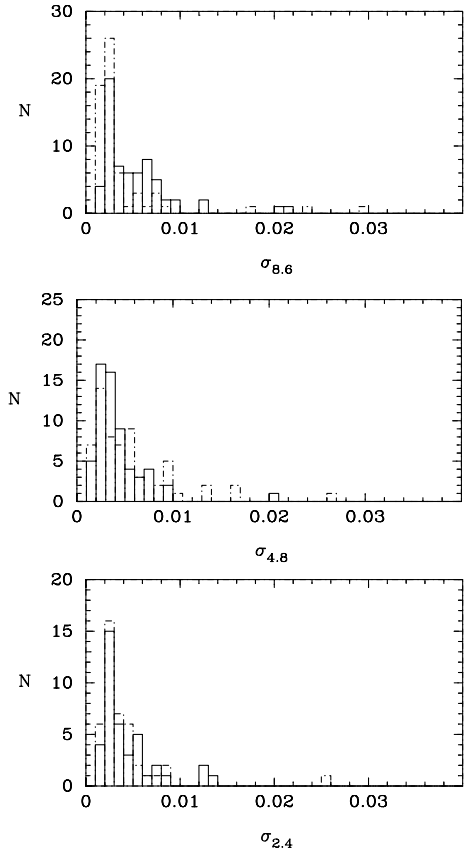

Figure 6. The number distribution of the rms in polarized flux densities at 8.6, 4.8 and 2.3 GHz from top to bottom.

6.2 Intrinsic versus extrinsic IDV

The suggested interpretations of IDV fall into two categories: processes intrinsic and extrinsic to the sources. The first possibility is difficult to accept for the extremely strong and rapid variability in sources such as PKS 0405−385, which imply the brightness temperature as high as $T_{\rm var} \sim 10^{21}$ K (Kedziora-Chudczer et al. 1997).

The variability brightness temperature, $T_{\rm var}$, can be reduced by postulating relativistic beaming δ. In the most extreme cases one has to invoke $\delta > 100$, which is difficult to justify on the theoretical (Begelman, Rees & Sikora 1994) and statistical grounds. The alternative idea of the intrinsic brightness temperature $T_{\rm b}$ actually exceeding the Compton scattering limit for the duration of an IDV event is yet to be fully explored.

Interpretation of IDV in terms of propagation-based flux density changes can often avoid a problem of the high brightness temperature, as it puts less stringent limits on the size of the source. Two most often considered propagation effects are microlensing (Quirrenbach et al. 1991) and interstellar scintillations (Rickett 1990).

The typical time-scales (>1 d) observed for IDV sources are consistent with microlensing in the presence of superluminal transverse velocities between the lens and the source, which could arise as a result of superluminal motion in the source (Gopal-Krishna & Subramanian 1991). However, to explain the observed hourly IDV over a few months arising from microlensing events, one would also expect an optical depth for lensing high enough to cause gravitational multiple imaging of IDV sources with a few arcsec separation, which has not been observed in any of these sources.

Models based on interstellar scintillation generally require less

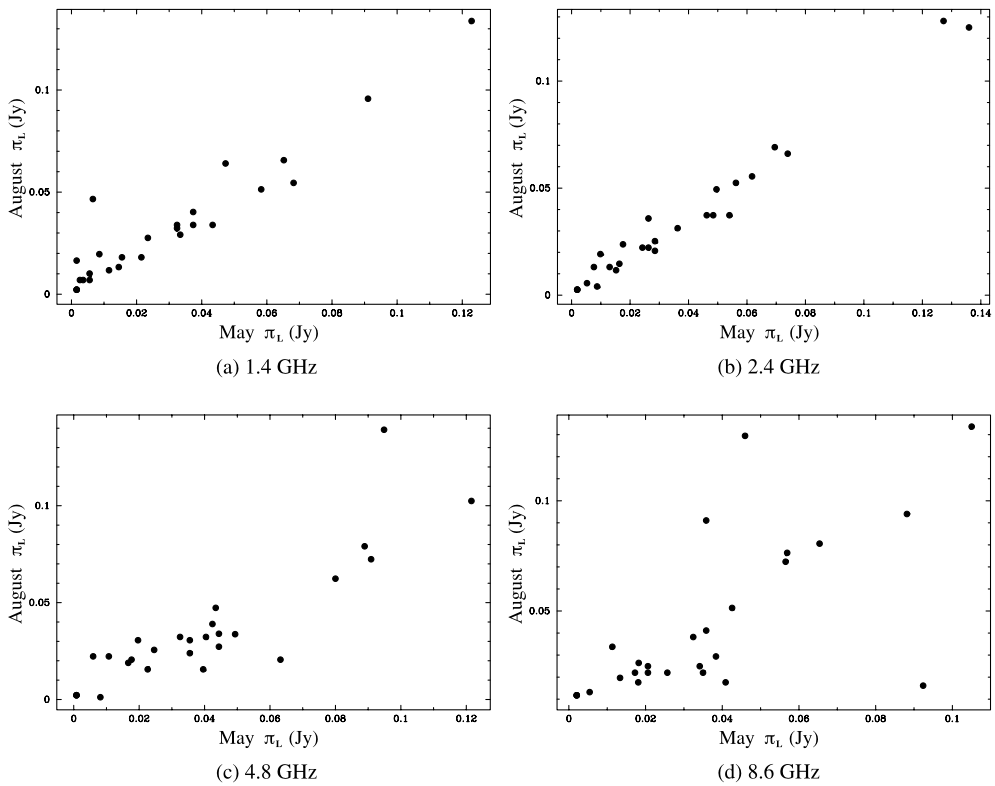

Figure 7. Scatter plot of the average polarized flux density in 1994 May versus August for all frequencies.

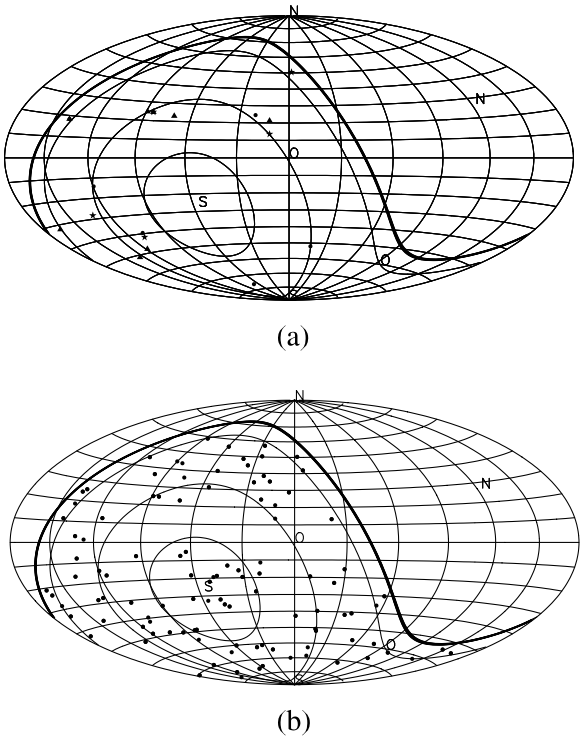

Figure 8. (a) Distribution of IDV sources with respect to the Galactic plane. Different symbols correspond to sources that show the strongest variability at different frequencies: stars (8.6 GHz), triangles (4.8 GHz) and dots (2.4 GHz). (b) Distribution of the whole sample in the Galactic coordinates. Data points are shown for 1994 May at 4.8 GHz. Only sources satisfying 'point-likeness' criteria (see Table 3) were included. The 1.4-GHz data are not included here owing to the larger uncertainties in flux density measurements. The thick curve shows the limits of the Survey, $\delta = +10°$.

extreme brightness temperatures in the IDV source because the source size is determined from the Fresnel scale requirements rather than from the variability time-scale. IDV in terms of ISS was discussed extensively by Rickett et al. (1995). Their model agreed well with the observed features of the data for the BL Lac S5 0917+624 under the assumption that the source diameter decreases with increasing frequency. The main complication of the ISS model was an interpretation of the polarized flux-density variability, which required the two-component source model with nearly orthogonal polarization angles of both components (Rickett et al. 1995).

Taking account of the complex source structure and the little-known structure of the scattering medium, it is not surprising that it is difficult to make very detailed models of ISS-induced IDV. Improved VLBI imaging may reveal more about the very inner structure of the radio sources, and the galactic multi-wavelength surveys will provide more detailed information about the ISM. The additional complexity is introduced by the presence of both extrinsic and intrinsic IDV occurring at the same time.

We have applied the ISS model to the variability of our most extreme IDV sources: PKS 0405−385 (Kedziora-Chudczer et al. 1997) and PKS 1519−273 (Macquart et al. 2000). The spectrum of modulation indices and the time-scales of variability are consistent with the model. However ISS interpretation fails to bring the T_B down below the 10^{12} K for these sources. Coherent emission processes are often thought of as an alternative interpretation of IDV because they can produce almost arbitrary high brightness temperature (Benford 1992; Lesch & Pohl 1992). Yet the large number density of Langmuir photons required in any such process in the small volumes inferred for the IDV sources induces higher order scattering effects, which reduce the efficiency of escaping radiation (Melrose 1998).

Nevertheless one should remain open to the possibility of non-synchrotron emission in inner regions of AGN, in view of the problems not only with explanation of inferred brightness temperatures, $T_{var} \sim 10^{21}$ K for the IDV sources, but also in view of the growing number sources with $T_B > 10^{12}$ K directly observed with the VLBI and VSOP (Linfield et al. 1989).

7 CONCLUSION

The ATCA IDV Survey provided a new sample of IDV sources. We examined the variability dependence on the morphology, spectral features and position of these sources with respect to the Galactic plane.

The IDV sources found in the ATCA Survey seem to be marginally less common than suggested in previous studies (see e.g. Quirrenbach et al. 1992, who claim that about 25 per cent of sources from their sample show variations larger than 2 per cent). We find that IDV is also present in the polarized flux density.

IDV appears to be transient in a large fraction of sources. However, we also find continuously variable sources, with the best examples being PKS 1519−273, PKS 1034−293 and PKS 1144−379 (Kedziora-Chudczer et al. 1998).

The long-term behaviour of IDV sources was studied by comparing the flux densities measured in two different observing sessions separated by 3 months. It appears that IDV sources do vary strongly on the time-scale of months. This property can be potentially used in search for the IDV sources.

The IDV variability observed in the ATCA Survey is not correlated with the strength of radio emission and only weakly correlated with spectral characteristics. The distribution of the IDV sources with respect to the Galactic plane is not random but understandably does not follow the simple predictions of ISS theory.

The ATCA IDV Survey was a systematic step towards an understanding of the IDV phenomenon. Although at present it is not possible to choose between competing interpretations of IDV on a purely statistical basis, the ongoing study of individual IDV sources discovered in the Survey will help to achieve this purpose.

ACKNOWLEDGMENTS

The Australia Telescope is funded by the Commonwealth Government for operation as a national facility by the CSIRO.

REFERENCES

Allen W. H. et al., 1993, Phys. Rev. D, 48, 466
Aller H. D., Aller M. F., Latimer G. E., Hodge P. E., 1985, ApJS, 59, 513
Begelman M. C., Rees M. J., Sikora M., 1994, ApJ, 429, L57
Benford G., 1992, ApJ, 391, L59
Duncan R. A., White G. L., Wark R., Reynolds J. E., Jauncey D. L., Norris R. P., Taaffe L., 1993, PASA, 10, 310
Gopal-Krishna, Subramanian K., 1991, Nat, 349, 766
Heeschen D. S., 1984, AJ, 89, 1111
Heeschen D. S., Krichbaum T., Schalinski C. J., Witzel A., 1987, AJ, 94, 1493
Jauncey D., Batty M., Gulkis S., Savage A., 1982, AJ, 87, 763
Jennison R. C., 1958, MNRAS, 118, 276

Kedziora-Chudczer L. L., 1998, PhD thesis, Univ. Sydney
Kedziora-Chudczer L. L., Jauncey D. L., Wieringa M. H., Walker M. A., Nicolson G. D., Reynolds J. E., Tzioumis A. K., 1997, ApJ, 490, L9
Kedziora-Chudczer L. L., Jauncey D. L., Wieringa M. H., Reynolds J. E., Tzioumis A. K., 1998, Conf. Proc. IAU 164. 271
Kedziora-Chudczer L. L., Jauncey D. L., Wieringa M., Macquart J.-P., Tzioumis A., Bignall H., 2000, in Schilizzi R. T., Vogel S. N., Paresce F., Elvis M. S., eds, IAU Symp. No. 205, Galaxies and their constituents at the highest angular resolution. Astron. Soc. Pac., San Francisco, in press
Kellermann K. I., Owen F. N., 1988, in Verschuur G. L., Kellermann K. I., eds, Galactic and Extragalactic Radio Astronomy. Springer-Verlag, New York, p. 581
Kellermann K. I., Pauliny-Toth I. I. K., 1969, ApJ, 155, L71
Kochanev P. Y., Gabuzda D. C., 1998, in Zensus J. A., Taylor G. B., Wrobel J. M., eds, IAU Colloq. 164, ASP Conf. Ser. Vol. 144. Astron. Soc. Pac., San Francisco, p. 273
Lesch H., Pohl M., 1992, A&A, 254, 29
Linfield R. P. et al., 1989, ApJ, 336, 1105
Macquart J.-P., Kedziora-Chudczer L. L., Rayner D. P., Jauncey D. L., 2000, ApJ, 538, 623
Mattox J. R., Wagner S. J., Malkan M., McGlynn T. A., Schachter J. F., Grove J. E., Johnson W. N., Kurfess J. D., 1997, ApJ, 476, 692
Melrose D. B., 1998, Ap&SS, 264, 391
Narayan R., 1992, Phil. Trans. R. Soc. Lond., 341, 151
Pesce J. E. et al., 1997, ApJ, 486, 770
Quirrenbach A., Witzel A., Qian S. J., Krichbaum T. P., Hummel C. A., Alberdi A., 1989, A&A, 226, L1
Quirrenbach A. et al., 1991, ApJ, 372, L71
Quirrenbach A. et al., 1992, A&A, 258, 279
Rickett B. J., 1990, ARA&A, 28, 561
Rickett B. J., Quirrenbach A., Wegner R., Krichbaum T. P., Witzel A., 1995, A&A, 293, 479
Sinclair M. W., Gough R. G., 1991, Int. Proc. IREECON '91. The IREE Australia, College of Electrical Engineering, p. 381
Taylor J. H., Cordes J. M., 1993, ApJ, 430, 467
Urry C. M., Padovani P., 1995, PASP, 107, 803
van der Laan H., 1966, Nat, 211, 1131
Wagner S. J., Witzel A., 1995, ARA&A, 33, 163
Walker M. A., 1998, MNRAS, 294, 307
Wegner R. G., 1994, PhD thesis, Univ. Bonn
Witzel A., Heeschen D. S., Schalinski C. J., Krichbaum T. P., 1986, Mitt. Astron. Ges., 65, 239

This paper has been typeset from a TEX/LATEX file prepared by the author.